

Project THEMIS
Technical Report No. 7

STRATIFIED FLOW OVER AN OBSTACLE;
A NUMERICAL EXPERIMENT

by

Jung-Tai Lin

and

C. J. Apelt

Prepared Under

Office of Naval Research

Contract No. N00014-68-A-0493-0001

Project No. NR 062-414/6-6-68(Code 438)

U.S. Department of Defense

Washington, D. C.

"This document has been approved for public release
and sale; its distribution is unlimited."

Fluid Dynamics and Diffusion Laboratory
College of Engineering
Colorado State University
Fort Collins, Colorado

January 1970

CER69-70JTL-CJA25



U18401 0575528

ABSTRACT

Numerical studies of time-dependent, two-dimensional, stratified flow of incompressible, viscous, diffusive fluid are described. The particular physical problem which has been considered is that of stratified flow over a vertical fence when the motion is impulsively started from rest. Solutions have been calculated for the following two cases: $R_e = 397$, $P_r = 10$, $R_i = 1.58$; and $R_e = 5000$, $P_r = 1$, $R_i = 1.58$. The results are presented as contour plots of the flow variables, generated directly by the computer. A new iterative method was used for numerical integration of the governing equations and was found to be very effective. The method is based on the combination of the Crank-Nicolson method with a strongly implicit iterative method developed by Stone (1968). Full details of the method are given together with a summary of its performance on the problems calculated. It is shown that proper treatment of the inflow and outflow boundary conditions is crucial for successful numerical modeling of stratified flows.

ACKNOWLEDGMENT

Acknowledgment is made to the National Center for Atmospheric Research, which is sponsored by the National Science Foundation, for use of its Control Data 6600 computer, and to the financial support by THEMIS Project under the grant N00014-68-A-0493-0001. Thanks are due to Dr. J. E. Cermak for his continuous encouragement during this research period.

LIST OF FIGURES

<u>Figure</u>		<u>Page</u>
1	Sketch of Grid Points, and Mesh Sizes	59
2	Sketch of Mesh in Vicinity of the Vertical Fence	59
3	Sketch of Interior Field and Boundaries of Stratified Flow Problem.	60
4	Sketch of Interior Field and Boundary of the Test Problem	61
5	Error Propagation for the Test Problem.	62
6	Flow Chart for Initial Solution	63
7	Flow Chart for Transient Solution	64
8	Stream Function at $t = 0.03$, $Re = 397$, $Pr = 10$, $Ri = 1.58$, $\Delta X = 0.25$, $\Delta Z = 0.25$, $\Delta t = 0.03$, grid points (180 x 30)	65
9	Flow Patterns at $t = 1.82$, $Re = 397$, $Pr = 10$, $Ri = 1.58$, $\Delta X = 0.25$, $\Delta Z = 0.25$, $\Delta r = 0.20$, grid points (180 x 30)	66
10	Flow Patterns at $t = 4.76$, $Re = 397$, $Pr = 10$, $Ri = 1.58$, $\Delta X = 0.25$, $\Delta Z = 0.25$, $\Delta t = 0.20$, grid points (180 x 30)	67
11	Flow Patterns at $t = 20.52$, $Re = 397$, $Pr = 10$, $Ri = 1.58$, $\Delta X = 0.25$, $\Delta Z = 0.25$, $\Delta t = 0.22$, grid points (180 x 30)	68
12	Flow Patterns at $t = 9.8$, $Re = 397$, $Pr = 10$, $Ri = 1.58$, $\Delta X = 0.25$, $\Delta Z = 0.25$, $\Delta t = 0.20$, grid points (180 x 30)	69
13	Flow Patterns at $t = 12.74$, $Re = 397$, $Pr = 10$, $Ri = 1.58$, $\Delta X = 0.25$, $\Delta Z = 0.25$, $\Delta t = 0.20$, grid points (180 x 30)	70
14	Flow Patterns at $t = 15.68$, $Re = 397$, $Pr = 10$, $Ri = 1.58$, $\Delta X = 0.25$, $\Delta Z = 0.25$, $\Delta t = 0.20$, grid points (180 x 30)	71
15	Stream Function at $t = 0.03$, $Re = 5000$, $Pr = 1$, $Ri = 1.58$, $\Delta X = 0.25$, $\Delta Z = 0.25$, $\Delta t = 0.03$, grid points (180 x 30)	72

LIST OF FIGURES - Continued

<u>Figure</u>		<u>Page</u>
16	Flow Patterns at $t = 2.88$, $Re = 5000$, $Pr = 1$, $Ri = 1.58$, $\Delta X = 0.25$, $\Delta Z = 0.25$, $\Delta t = 0.22$, grid points (180 x 30)	73
17	Flow Patterns at $t = 8.34$, $Re = 5000$, $Pr = 1$, $Ri = 1.58$, $\Delta X = 0.25$, $\Delta Z = 0.25$, $\Delta t = 0.22$, grid points (180 x 30)	74
18	Flow Patterns at $t = 13.38$, $Re = 5000$, $Pr = 1$, $Ri = 1.58$, $\Delta X = 0.25$, $\Delta Z = 0.25$, $\Delta t = 0.22$, grid points (180 x 30)	75
19	Flow Patterns at $t = 18.42$, $Re = 5000$, $Pr = 1$, $Ri = 1.58$, $\Delta X = 0.25$, $\Delta Z = 0.25$, $\Delta t = 0.22$, grid points (180 x 30) ;	76
20	Flow Patterns at $t = 20.52$, $Re = 5000$, $Pr = 1$, $Ri = 1.58$, $\Delta X = 0.25$, $\Delta Z = 0.25$, $\Delta t = 0.22$, grid points (180 x 30)	77
21	Flow Patterns at $t = 23.46$, $Re = 5000$, $Pr = 1$, $Ri = 1.58$, $\Delta X = 0.25$, $\Delta Z = 0.25$, $\Delta t = 0.22$, grid points (180 x 30)	78

TABLE OF CONTENTS

<u>Chapter</u>		<u>Page</u>
	ABSTRACT	ii
	ACKNOWLEDGMENT	iii
I	INTRODUCTION	1
II	GOVERNING EQUATIONS AND BOUNDARY CONDITIONS.	4
	2.1 Governing Equations in Differential Form.	4
	2.2 Governing Equations in Finite Difference Form	6
	2.3 Initial and Boundary Conditions	12
III	ITERATIVE METHOD	20
	3.1 Statement of Problem.	20
	3.2 Algorithm for Iteration	23
	3.3 Convergence Rate.	29
IV	COMPUTATIONAL PROCEDURE.	38
V	RESULTS AND DISCUSSION	43
	BIBLIOGRAPHY	55
	FIGURES.	58

Chapter I

INTRODUCTION

When stably stratified air flows over an obstacle, air currents tend to follow a wave-like pattern in the lee side of the obstacle. This phenomenon, called mountain lee-waves, has been observed in the atmosphere (Holmboe and Klieforth, 1957). Lee-waves have been studied analytically with the help of perturbation theory for steady lee-waves of small amplitudes (Lyra, 1943; Queney, 1947; Scorer, 1949). For a particular boundary condition upstream, $\sqrt{\rho} u = \text{constant}$, where ρ is the fluid density and u is the streamwise velocity, a nonlinear model for steady lee-waves of finite amplitude was investigated by Long (1953), Yih (1960), Pao (1967), and Miles (1968, 1969).

These analytical approaches have contributed significantly to the understanding of lee-wave phenomena. However, in nature, lee-wave flows usually involve waves of finite amplitude and, in addition, the boundary conditions are complicated. Moreover, the flow may be in a transient state. Hence, for a better understanding of lee-wave phenomena, laboratory simulation and numerical modeling with a computer are the only approaches currently available apart from prototype study by field investigation. Laboratory simulations have been conducted by Long (1959) with a liquid model, and by Lin and Binder (1967) in a wind tunnel.

In laboratory simulation, one usually encounters limitations in the variability of flow parameters such as flow velocity and stratification. In particular, Reynolds numbers are usually quite low when high Froude numbers (or low Richardson numbers) are required. Consequently, molecular effects are inevitable and greatly influence the flow patterns and

simulation analysis becomes difficult. As far as numerical computation is concerned, a numerical simulation by computer is usually possible provided a stable and rapidly convergent scheme is available. Nevertheless, a numerical computation itself is by no means a trivial and straightforward manipulation. In particular, when a nonlinear partial differential equation such as the Navier-Stokes equation is involved, a numerical experiment judged with physical understanding is always needed because rigorous analyses of computational stability, convergence, and error propagation are not available yet, although some approximate analyses based on the existing mathematical theories have been explored. Therefore, our understanding will be greatly dependent on the numerical experiment coupled with these approximate analyses. However, even though the results of a numerical simulation may be comparable to those of laboratory experiments, a numerical simulation is still desirable since the flow parameters can be varied with such ease and then more information is available. Of course, one must recognize that, because of the limitation in the available computer storage and because of the difficulty in generating turbulence by computer, three-dimensional problems associated with turbulence must still be studied in the laboratory or by prototype investigations.

Numerical studies of lee-waves have been carried out by Hovermale (1965) and by Foldvik and Wurtele (1967). Both studies treated the transient flow of inviscid stratified fluid over a barrier as an initial value problem. For the lack of suitable boundary conditions, both upstream and downstream, cyclic boundary conditions were used, i.e., the calculated flow conditions downstream of the barrier were fed back

in upstream as the oncoming flow towards the barrier. Some important features concerning the nonlinear effects on lee-waves were obtained.

In the numerical experiment described in this report, two-dimensional laminar motion of an incompressible, viscous, diffusive and nonhomogeneous fluid over an obstacle will be studied. The fruitful results from the studies by Hovermale and by Foldvik and Wurtele indicate that treating a transient flow instead of a steady flow is a helpful approach from the numerical point of view and, thus, in this numerical study a transient flow is considered. However, we shall abandon the cyclic boundary condition and make a detailed study of the effects of boundary conditions on the computation. In addition, a new iterative method is introduced in order to increase the speed of the computation.

Chapter II

GOVERNING EQUATIONS AND BOUNDARY CONDITIONS

2.1 Governing Equations

Consider two-dimensional laminar motion of an incompressible, viscous, diffusive and nonhomogeneous fluid in a uniform gravitational field. The fluid properties other than the density, such as the viscosity μ_0 and thermal conductivity k_0 , are assumed to be uniform in the flow field. By using Boussinesq approximation, the equations of motion, the continuity equation, and the equation of energy are formulated as follows:

$$\rho_0 \left(\frac{\partial \tilde{u}}{\partial \tilde{t}} + \tilde{u} \frac{\partial \tilde{u}}{\partial \tilde{x}} + \tilde{w} \frac{\partial \tilde{u}}{\partial \tilde{z}} \right) = - \frac{\partial \tilde{p}}{\partial \tilde{x}} + \mu_0 \tilde{\nabla}^2 \tilde{u} \quad , \quad (2.1)$$

$$\rho_0 \left(\frac{\partial \tilde{w}}{\partial \tilde{t}} + \tilde{u} \frac{\partial \tilde{w}}{\partial \tilde{x}} + \tilde{w} \frac{\partial \tilde{w}}{\partial \tilde{z}} \right) = - \frac{\partial \tilde{p}}{\partial \tilde{z}} - \tilde{\rho} g + \mu_0 \tilde{\nabla}^2 \tilde{w} \quad , \quad (2.2)$$

$$\frac{\partial \tilde{u}}{\partial \tilde{x}} + \frac{\partial \tilde{w}}{\partial \tilde{z}} = 0 \quad , \quad (2.3)$$

and

$$\rho_0 C_p \left(\frac{\partial \tilde{T}}{\partial \tilde{t}} + \tilde{u} \frac{\partial \tilde{T}}{\partial \tilde{x}} + \tilde{w} \frac{\partial \tilde{T}}{\partial \tilde{z}} \right) = k_0 \tilde{\nabla}^2 \tilde{T} \quad , \quad (2.4)$$

where \tilde{u} and \tilde{w} are the velocity components in the Cartesian coordinates \tilde{x} and \tilde{z} , $\tilde{\rho}$ is the density, ρ_0 is the reference density, \tilde{p} is the pressure, C_p is the specific heat capacity at constant pressure, \tilde{T} is the temperature, \tilde{t} is the time, and $\tilde{\nabla}^2 = \partial^2/\partial \tilde{x}^2 + \partial^2/\partial \tilde{z}^2$ is the Laplacian operator. In Equation (2.4) the heat dissipation due to molecular viscosity is neglected.

By cross differentiating Equations (2.1) and (2.2) and then eliminating the pressure, one arrives at the vorticity transport equation,

$$\left(\frac{\partial \tilde{\zeta}}{\partial \tilde{t}} + \tilde{u} \frac{\partial \tilde{\zeta}}{\partial \tilde{x}} + \tilde{w} \frac{\partial \tilde{\zeta}}{\partial \tilde{z}} \right) = \frac{1}{T_0} \frac{\partial \tilde{T}}{\partial \tilde{x}} g + \nu \tilde{\nabla}^2 \tilde{\zeta} , \quad (2.5)$$

where $\nu = \mu_0 / \rho_0$ is the kinematic viscosity, the vorticity $\tilde{\zeta}$ is defined by

$$\tilde{\zeta} = \partial \tilde{w} / \partial \tilde{x} - \partial \tilde{u} / \partial \tilde{z} , \quad (2.6)^*$$

and $\frac{1}{T_0} \frac{\partial \tilde{T}}{\partial \tilde{x}} = - \frac{1}{\rho_0} \frac{\partial \tilde{\rho}}{\partial \tilde{x}}$ has resulted from use of the equation of state for the incompressible fluid and of the Boussinesq approximation. A stream function, $\tilde{\psi}$, which satisfies the continuity equation (2.3) is introduced as

$$\tilde{u} = \partial \tilde{\psi} / \partial \tilde{z} , \quad \text{and} \quad \tilde{w} = - \partial \tilde{\psi} / \partial \tilde{x} , \quad (2.7)$$

and the vorticity can be redefined as

$$\tilde{\zeta} = - \tilde{\nabla}^2 \tilde{\psi} . \quad (2.8)$$

For convenience, Equations (2.5), (2.7), (2.8) together with Equation (2.4), presented in the form

$$\frac{\partial \tilde{T}}{\partial \tilde{t}} + \tilde{u} \frac{\partial \tilde{T}}{\partial \tilde{x}} + \tilde{w} \frac{\partial \tilde{T}}{\partial \tilde{z}} = \kappa \tilde{\nabla}^2 \tilde{T} , \quad (2.9)$$

* The sign convention for $\tilde{\zeta}$ is the opposite of that more commonly used. It is used here for convenience.

in which $\kappa = k_o/\rho C_p$ is the thermal diffusivity, will be normalized to give a set of nondimensional equations.

Let

$$\begin{aligned} u &= \tilde{u}/U, & w &= \tilde{w}/U, & t &= \tilde{t}/(L/U), & \zeta &= \tilde{\zeta}/(U/L), \\ x &= \tilde{x}/L, & z &= \tilde{z}/L, & T &= \frac{\tilde{T}-T_o}{\Delta T}, & R_e &= UL/\nu, & P_r &= \nu/\kappa, \\ \psi &= \tilde{\psi}/UL, & \text{and } F_r &= \frac{U}{\sqrt{gL \frac{\Delta T}{T_o}}} = \frac{1}{\sqrt{R_i}}. \end{aligned} \quad (2.10)$$

U , L , and ΔT are the characteristic velocity, length, and temperature difference, respectively, and R_e , P_r , F_r and R_i are the Reynolds number, Prandtl number, Froude number and Richardson number. The governing equations in dimensionless form become:

$$\frac{\partial \zeta}{\partial t} + u \frac{\partial \zeta}{\partial x} + w \frac{\partial \zeta}{\partial z} = R_i \frac{\partial T}{\partial x} + \frac{1}{R_e} \nabla^2 \zeta, \quad (2.11)$$

$$\frac{\partial T}{\partial t} + u \frac{\partial T}{\partial x} + w \frac{\partial T}{\partial z} = \frac{1}{P_r R_e} \nabla^2 T, \quad (2.12)$$

and

$$\zeta = -\nabla^2 \psi, \quad (2.13)$$

where

$$\nabla^2 = \frac{\partial^2}{\partial x^2} + \frac{\partial^2}{\partial z^2}.$$

2.2 Governing Equations in Finite Difference Form

For numerical computation, Equations (2.11), (2.12), and (2.13) will be discretized into stable and convergent finite difference forms

and then, provided the initial conditions, boundary conditions and parameters are adequately defined, one may simulate a flow with the computer.

In Equation (2.13) the derivatives are replaced by central differences to give,

$$\frac{\psi_{i+1,j} - 2\psi_{i,j} + \psi_{i-1,j}}{\Delta x^2} + \frac{\psi_{i,j+1} - 2\psi_{i,j} + \psi_{i,j-1}}{\Delta z^2} = -\zeta_{i,j} \quad (2.14)$$

where Δx and Δz are the mesh intervals in the horizontal and vertical directions, respectively, the subscripts i and j indicate the space coordinates by $x = i\Delta x$ and $z = j\Delta z$. Figure 1 displays the arrangement of the mesh. It can readily be shown that in respect to Equation (2.13), Equation (2.14) has a truncation error $\epsilon = O(\Delta x^2) + O(\Delta z^2)$ where the notation O denotes that $\lim_{\delta \rightarrow 0} \frac{O(\delta)}{\delta}$ is finite. Thus, the smaller the mesh size is, the smaller the truncation error will be.

Discretization of Equations (2.11) and (2.12) presents greater difficulty since one must consider questions of convergence and of stability. If a finite difference scheme has the property of stability, the difference between the solution of the finite difference system, say $\theta_{i,j,k}$, and the exact solution of the differential system, say $\theta(i\Delta x, j\Delta z, k\Delta t)$, will remain bounded as time increases indefinitely for fixed mesh sizes, Δx , Δz and time increment Δt . Convergence guarantees that, for t fixed, $\theta_{i,j,k}$ will converge to $\theta(i\Delta x, j\Delta z, k\Delta t)$ as Δx , Δz , and Δt approach to zero. A further difficulty arises from the nonlinearity involved in the coupling between Equations (2.11) and (2.13). Experience shows that the nonlinearity can produce instability in the computations although stability analysis based on the locally

linearized finite difference system indicates a stable scheme. For this reason numerical experiments are always needed.

Generally speaking, there are two classes of schemes, explicit and implicit, for solving a transient problem. In explicit schemes the solution at a given grid point for the new time level can be calculated from known quantities at the present or previous time level. On the other hand, implicit schemes involve the solution of a set of simultaneous equations for calculating the solution at all the grid points at the new time level. Obviously, explicit schemes involve less algebraic manipulations than do implicit schemes. However, for a linear system, stability analysis shows that the time increment Δt for explicit schemes is restricted and usually Δt is kept small to satisfy requirements of stability and of convergence; whereas, in implicit schemes the time interval has no restrictions except those imposed by considerations of accuracy. Consequently, a larger time increment can be used with implicit schemes and this can result in less computer time being required than in the case of explicit schemes. In particular, if we are chiefly interested in the asymptotic solution of a transient flow, implicit schemes appear to be preferable to explicit schemes. Here we would point out that the computational scheme which is best for a given problem will often be determined by the nature of the physical phenomena. For instance, if a flow involves phenomena of short period or high frequency the time increment must be considerably shorter than this period. An example is the numerical calculation of vortex shedding phenomena behind an obstacle (Fromm and Harlow, 1963; Thoman and Szweczyk, 1966). And, of course, the mesh size must be considerably less than the characteristic length of the shedding vortex. As for

the present numerical investigation, we shall use an implicit scheme since transient lee-waves propagate slowly and have a characteristic length comparable to or larger than the obstacle height or width.

Even when an implicit scheme is used, the nonlinearity of the equations can cause difficulties when the Reynolds number Re becomes large. If the convective terms of Equation (2.11) are discretized with central space differences, the off-diagonal terms of the amplification matrix of the difference equations can become large in magnitude compared to the principal diagonal terms as Re increases and, then, the absolute values of the eigenvalues of the amplification matrix may be greater than unity. This situation has been improved somewhat by use of the alternating direction implicit (ADI) method (Peaceman and Rachford, 1955) for moderate Reynolds numbers (Pearson, 1965). For higher Reynolds numbers, the backward and forward difference method for convective terms has proved to be very effective (Thoman and Szewczyk, 1966). This method was first suggested by Lelevier (Richtmyer and Morton, 1967) and consists in representing $\partial\zeta/\partial x$ (or $\partial\zeta/\partial z$) by the backward or forward finite difference depending on whether u (or w) is positive or negative. In this way, the amplification matrix is made positive definite and diagonally dominant; thus, the absolute values of the eigenvalues of the amplification matrix are less than unity and the stability criterion becomes weakly dependent on the Reynolds number. This method together with the ADI method has been used by Pao (1969) for calculation of homogeneous flow of a viscous incompressible fluid over a horizontal flat plate of finite length.

In the present study, for high Reynolds number this backward and forward difference method is applied to the convective terms and then

the Crank-Nicolson implicit scheme is used. The governing equations in finite difference form are formulated as follows:

(i) Temperature field:

$$\begin{aligned}
& \frac{T_{i,j}^{n+1} - T_{i,j}^n}{\Delta t} + \frac{u_{i,j}^n}{2} \left[A_2 \frac{T_{i,j}^{n+1} - T_{i-1,j}^{n+1} + T_{i,j}^n - T_{i-1,j}^n}{\Delta x} \right. \\
& + A_3 \frac{T_{i+1,j}^{n+1} - T_{i,j}^{n+1} + T_{i+1,j}^n - T_{i,j}^n}{\Delta x} \left. \right] \\
& + \frac{w_{i,j}^n}{2} \left[A_4 \frac{T_{i,j}^{n+1} - T_{i,j-1}^{n+1} + T_{i,j}^n - T_{i,j-1}^n}{\Delta z} \right. \\
& + A_5 \frac{T_{i,j+1}^{n+1} - T_{i,j}^{n+1} + T_{i,j+1}^n - T_{i,j}^n}{\Delta z} \left. \right] \\
& = \frac{1}{2P_{rRe}} \left[\frac{T_{i+1,j}^{n+1} - 2T_{i,j}^{n+1} + T_{i-1,j}^{n+1} + T_{i+1,j}^n - 2T_{i,j}^n + T_{i-1,j}^n}{\Delta x^2} \right. \\
& + \left. \frac{T_{i,j+1}^{n+1} - 2T_{i,j}^{n+1} + T_{i,j-1}^{n+1} + T_{i,j+1}^n - 2T_{i,j}^n + T_{i,j-1}^n}{\Delta z^2} \right], \quad (2.15)
\end{aligned}$$

(ii) Vorticity field:

$$\begin{aligned}
& \frac{\zeta_{i,j}^{n+1} - \zeta_{i,j}^n}{\Delta t} + \frac{u_{i,j}^n}{2} \left[A_2 \frac{\zeta_{i,j}^{n+1} - \zeta_{i-1,j}^{n+1} + \zeta_{i,j}^n - \zeta_{i-1,j}^n}{\Delta x} \right. \\
& \left. + A_3 \frac{\zeta_{i+1,j}^{n+1} - \zeta_{i,j}^{n+1} + \zeta_{i+1,j}^n - \zeta_{i,j}^n}{\Delta x} \right] \\
& + \frac{w_{i,j}^n}{2} \left[A_4 \frac{\zeta_{i,j}^{n+1} - \zeta_{i,j-1}^{n+1} + \zeta_{i,j}^n - \zeta_{i,j-1}^n}{\Delta z} \right. \\
& \left. + A_5 \frac{\zeta_{i,j+1}^{n+1} - \zeta_{i,j}^{n+1} + \zeta_{i,j+1}^n - \zeta_{i,j}^n}{\Delta z} \right] \\
& = \frac{1}{2R_e} \left[\frac{\zeta_{i+1,j}^{n+1} - 2\zeta_{i,j}^{n+1} + \zeta_{i-1,j}^{n+1} + \zeta_{i+1,j}^n - 2\zeta_{i,j}^n + \zeta_{i-1,j}^n}{\Delta x^2} \right. \\
& \left. + \frac{\zeta_{i,j+1}^{n+1} - 2\zeta_{i,j}^{n+1} + \zeta_{i,j-1}^{n+1} + \zeta_{i,j+1}^n - 2\zeta_{i,j}^n + \zeta_{i,j-1}^n}{\Delta z^2} \right] \\
& + \frac{R_i}{4} \left[\frac{T_{i+1,j}^{n+1} - T_{i-1,j}^{n+1} + T_{i+1,j}^n - T_{i-1,j}^n}{\Delta x} \right], \tag{2.16}
\end{aligned}$$

and

(iii) Stream function field:

$$\frac{\psi_{i+1,j} - 2\psi_{i,j} + \psi_{i-1,j}}{\Delta x^2} + \frac{\psi_{i,j+1} - 2\psi_{i,j} + \psi_{i,j-1}}{\Delta z^2} = -\zeta_{i,j} \quad , \quad (2.17)$$

in which

$$\begin{aligned} \text{(a)} \quad A_2 &= 1 \quad , \quad A_3 = 0 \quad \text{for } u_{i,j}^n \geq 0 \quad , \\ \text{(b)} \quad A_2 &= 0 \quad , \quad A_3 = 1 \quad \text{for } u_{i,j}^n < 0 \quad , \\ \text{(c)} \quad A_4 &= 1 \quad , \quad A_5 = 0 \quad \text{for } w_{i,j}^n \geq 0 \quad , \\ \text{and (d)} \quad A_4 &= 0 \quad , \quad A_5 = 1 \quad \text{for } w_{i,j}^n < 0 \quad . \end{aligned} \quad (2.18)$$

In Equations (2.15) and (2.16), the superscripts $n+1$ and n denote the time steps $(n+1)\Delta t$ and $n\Delta t$. In the course of calculation the quantities at the n th time step are known, while those at the $(n+1)$ time step are unknown and must be calculated.

2.3 Initial and Boundary Conditions

In the atmosphere, flow conditions may vary from time to time and we may use observed data as the initial conditions and calculate the flow as it develops from that state. However, this makes the problem complicated and, in this numerical experiment we consider a simpler condition. Consider a vertical fence of infinitesimal thickness and height $2L$ in a fluid of unlimited extent. The fluid, initially uniformly stratified in the vertical direction and at rest, is impulsively accelerated in the horizontal direction so that the velocity far from

the fence is U and, thereafter, the velocity is maintained constant. The flow is initially irrotational and the vorticity which is generated as a result of the no-slip boundary condition on the vertical fence is concentrated only on the fence. As time passes, vorticity spreads into the flow field under the combined action of viscous diffusion and of convection. The temperature distribution at the initial instant when the flow starts impulsively is linearly distributed with height and the temperature is constant along a streamline; the characteristic temperature difference is defined by $\Delta T = \tilde{T}_L - T_0$ where \tilde{T}_L is the temperature far upstream at height L measured from the center of the vertical fence. As time passes, the temperature distribution will be changed as a result of thermal diffusion and of convection.

As far as the boundary conditions are concerned, only the no-slip condition for a viscous fluid is clearly defined on the boundary of obstacle. However, the governing equations are expressed in terms of vorticity and the velocity is in turn calculated from the stream function equation; in other words, there is no a priori boundary condition available for vorticity. In the following, we express the vorticity on the obstacle boundary in terms of the vorticity and stream function in the neighborhood.

Referring to Figure 2, we express the stream function ψ_A at A in terms of the stream function ψ_B and its derivatives at B by a Taylor series expansion

$$\psi_A = \psi_B + \Delta x \left(\frac{\partial \psi}{\partial x} \right)_B + \frac{\Delta x^2}{2!} \left(\frac{\partial^2 \psi}{\partial x^2} \right)_B + \frac{\Delta x^3}{3!} \left(\frac{\partial^3 \psi}{\partial x^3} \right)_B + \frac{\Delta x^4}{4!} \left(\frac{\partial^4 \psi}{\partial x^4} \right)_B + O(\Delta x^5) \quad (2.19)$$

Equation (2.19) can be related to the vorticity and its derivatives at B by virtue of the no-slip boundary condition at B as

$$\psi_A = \psi_B - \frac{\Delta x^2}{2!} \zeta_B - \frac{\Delta x^3}{3!} \left(\frac{\partial \zeta}{\partial x} \right)_B - \frac{\Delta x^4}{4!} \left(\frac{\partial^2 \zeta}{\partial x^2} - \frac{\partial^2 \zeta}{\partial z^2} \right)_B + O(\Delta x^5) ,$$

which is then rewritten in the form

$$\begin{aligned} \zeta_B &= \frac{3}{\Delta x^2} (\psi_B - \psi_A) - \frac{1}{2} \zeta_A + \frac{\Delta x^2}{8} (\nabla^2 \zeta)_B + O(\Delta x^3) \\ &= \frac{3}{\Delta x^2} (\psi_B - \psi_A) - \frac{1}{2} \zeta_A + \frac{\Delta x^2}{8} R_e \left(\frac{\partial \zeta}{\partial t} \right)_B + O(\Delta x^3) \end{aligned} \quad (2.20)$$

by using the Taylor expansion of ζ_A about B and the no-slip condition. The same derivation was given by Hung (1966). Now, if $(\partial \zeta / \partial t)_B$ is expressed by

$$\left(\frac{\partial \zeta}{\partial t} \right)_B = \frac{\zeta_B^{n+1} - \zeta_B^n}{\Delta t}$$

and the remaining terms of the right hand side of Equation (2.20) are given the values corresponding to the nth time step, then we have

$$\begin{aligned} \zeta_B^{n+1} &= \frac{8\Delta t}{R_e \Delta x^2} \left[-\frac{3}{\Delta x^2} (\psi_B^n - \psi_A^n) + \frac{1}{2} \zeta_A^n + \zeta_B^n \left(1 + \frac{R_e \Delta x^2}{8\Delta t} \right) \right] \\ &+ O(\Delta x \Delta t) + O(\Delta t^2) . \end{aligned} \quad (2.21)$$

For the vorticity on the upstream face of the vertical fence, a similar equation is available:

$$\zeta_{B'}^{n+1} = \frac{8\Delta t}{R_e \Delta x^2} \left[-\frac{3}{\Delta x^2} (\psi_{B'}^n - \psi_{A'}^n) + \frac{1}{2} \zeta_{A'}^n + \zeta_{B'}^n \left(1 + \frac{R_e \Delta x^2}{8\Delta t} \right) \right] + O(\Delta x \Delta t) + O(\Delta t^2) \quad (2.22)$$

Hence the vorticity on the boundary of the vertical fence at the (n+1) time step can be evaluated from the quantities at the nth time step, and then is used as a boundary condition for the calculation of vorticity at interior points at the n+1 time step. In the case when an iterative process is used for the calculation of vorticity at a given time step, $\zeta_B^{(m+1)}$ and $\zeta_{B'}^{(m+1)}$ at the (m+1) iteration are calculated from the values of the mth iteration by,

$$\zeta_B^{(m+1)} = \frac{3}{\Delta x^2} (\psi_B^{(m)} - \psi_A^{(m)}) - \frac{1}{2} \zeta_A^{(m)} + O(\Delta x^2) \quad , \quad (2.23)$$

and

$$\zeta_{B'}^{(m+1)} = \frac{3}{\Delta x^2} (\psi_{B'}^{(m)} - \psi_{A'}^{(m)}) - \frac{1}{2} \zeta_{A'}^{(m)} + O(\Delta x^2) \quad . \quad (2.24)$$

Subsequently they are used as boundary conditions for calculating vorticity at interior points at the (m+1) iteration.

As for the boundary value of vorticity on the corner of the vertical fence, C, a different expression is derived as follows. Expanding the vorticities ζ_E , $\zeta_{E'}$, ζ_D , and ζ_F in Taylor series about C, we have

$$-2\zeta_D + \zeta_F = -\zeta_C + \Delta z^2 \left(\frac{\partial^2 \zeta}{\partial z^2} \right)_C + O(\Delta z^3) \quad ,$$

and

$$\zeta_E + \zeta_{E'} = 2\zeta_C + \Delta x^2 \left(\frac{\partial^2 \zeta}{\partial x^2} \right)_C + O(\Delta x^3) ,$$

which, for $\Delta x = \Delta z$, are combined to give,

$$\begin{aligned} \zeta_C &= - 2\zeta_D + \zeta_F + \zeta_E + \zeta_{E'} - \Delta x^2 (\nabla^2 \zeta)_C + O(\Delta x^3) \\ &= - 2\zeta_D + \zeta_F + \zeta_E + \zeta_{E'} - \Delta x^2 R_e \left(\frac{\partial \zeta}{\partial t} \right)_C + O(\Delta x^3) . \end{aligned} \quad (2.25)$$

Hence, a finite difference form for Equation (2.25) is written as

$$\begin{aligned} \zeta_C^{n+1} &= \frac{\Delta t}{R_e \Delta x^2} \left[- 2\zeta_D^n + \zeta_F^n + \zeta_E^n + \zeta_{E'}^n - \zeta_C^n \right] \\ &+ \zeta_C^n + O(\Delta t^2) + O(\Delta x \Delta t) . \end{aligned} \quad (2.26)$$

For the iterative process we have simply

$$\zeta_C^{(m+1)} = - 2\zeta_D^{(m)} + \zeta_F^{(m)} + \zeta_E^{(m)} + \zeta_{E'}^{(m)} + O(\Delta x^2) . \quad (2.27)$$

As far as temperature distribution on the obstacle is concerned, we consider a uniform distribution for convenience, i.e., $\tilde{T} = T_0$ or $T = 0$.

On the outer boundary beyond the obstacle the boundary conditions are not defined a priori. Upstream very far from the obstacle, one may define a prescribed boundary condition. However, because of the presence of disturbances propagating from the obstacle both upstream and downstream, the boundary conditions for both inflow and outflow boundaries have to be defined in a less restrictive way by an extrapolation method derived from the Milne predictor formula,

$$y_{i+1} = y_{i-3} + \frac{4\Delta x}{3} (2y'_i - y'_{i-1} + 2y'_{i-2}) + O(\Delta x^5) , \quad (2.28)$$

where the prime denotes the derivative with respect to x and y is a function of x . By using the formulae

$$y'_i = \frac{1}{12\Delta x} (3y_{i-4} - 16y_{i-3} + 36y_{i-2} - 48y_{i-1} + 25y_i) + O(\Delta x^4) ,$$

$$y'_{i-1} = \frac{1}{12\Delta x} (-y_{i-4} + 6y_{i-3} - 18y_{i-2} + 10y_{i-1} + 3y_i) + O(\Delta x^4) ,$$

and

$$y'_{i-2} = \frac{1}{12\Delta x} (y_{i-4} - 8y_{i-3} + 8y_{i-1} - y_i) + O(\Delta x^4) ,$$

Equation (2.28) is formulated as

$$y_{i+1} = y_{i-4} - 5y_{i-3} + 10y_{i-2} - 10y_{i-1} + 5y_i + O(\Delta x^5) . \quad (2.29)$$

Hence, with an error of order Δx^5 , the stream function, vorticity, and temperature on the outflow boundary are expressed by extrapolating from the neighboring upstream points as follows:

$$\psi_{i+1,j} = \psi_{i-4,j} - 5\psi_{i-3,j} + 10\psi_{i-2,j} - 10\psi_{i-1,j} + 5\psi_{i,j} , \quad (2.30a)$$

$$\zeta_{i+1,j} = \zeta_{i-4,j} - 5\zeta_{i-3,j} + 10\zeta_{i-2,j} - 10\zeta_{i-1,j} + 5\zeta_{i,j} , \quad (2.30b)$$

and

$$T_{i+1,j} = T_{i-4,j} - 5T_{i-3,j} + 10T_{i-2,j} - 10T_{i-1,j} + 5T_{i,j} . \quad (2.30c)$$

A similar but different form was used by Hung (1966) successfully for a laminar flow in a conduit expansion. Similarly, these variables on the inflow boundary are expressed by extrapolating from the neighboring downstream points

$$\psi_{i-1,j} = \psi_{i+4,j} - 5\psi_{i+3,j} + 10\psi_{i+2,j} - 10\psi_{i+1,j} + 5\psi_{i,j} \quad , \quad (2.31a)$$

$$\zeta_{i-1,j} = \zeta_{i+4,j} - 5\zeta_{i+3,j} + 10\zeta_{i+2,j} - 10\zeta_{i+1,j} + 5\zeta_{i,j} \quad , \quad (2.31b)$$

and

$$T_{i-1,j} = T_{i+4,j} - 5T_{i+3,j} + 10T_{i+2,j} - 10T_{i+1,j} + 5T_{i,j} \quad . \quad (2.31c)$$

The detailed study of boundary conditions Equations (2.30) and (2.31) will be presented when the computational results are described.

For an exact simulation of flow over an obstacle by computer, the computation should cover the whole flow field 1234 (see Fig. 3), especially when some asymmetric flow patterns such as shedding vortices are present. These would be expected to occur when $\sigma = \frac{R_i^{1/2}}{\log R_e/40} < 1$, and $R_e > 40$ (Pao, 1968). However, because of the limitation of computer capacity, a flow field of half space 1256 was considered instead. It is assumed that the flow field is symmetric about the line 56. Actually this is not a bad assumption when $\sigma > 1$ according to Pao. Hence, we assume that when $t > 0$

$$\begin{aligned} \psi_{i,1} &= 0 \quad , \\ \zeta_{i,1} &= 0 \quad , \\ T_{i,1} &= 0 \quad , \quad \text{or} \quad \tilde{T}_{i,1} = T_0 \end{aligned} \quad (2.32)$$

for the boundary conditions on the line of symmetry, 56, and

$$\begin{aligned}w_{i,N} &= 0 \quad , \\ \zeta_{i,N} &= 0 \quad , \\ \partial/\partial x(T_{i,N}) &= 0\end{aligned}\tag{2.33}$$

for the upper boundary condition on the line 12.

Chapter III

ITERATION METHOD

In the numerical solution of Equations (2.15), (2.16), and (2.17) an iterative process is always encountered because of the boundary conditions and the nonlinearity of the equations. Iterative methods, such as the Gauss-Seidel process, SOR (successive over relaxation), or ADI (alternating direction implicit method) may be used. However, in this study a new strongly implicit iterative method proposed by Stone (1968) will be used. This method has several advantages over the methods previously used. Firstly, its rate of convergence does not depend strongly on the nature of the coefficient matrix of the equations to be solved; secondly, it is not sensitive to the choice of iteration parameter; and thirdly, it reduces significantly the computational effort.

3.1 Statement of Problem

There are many methods available for solving a set of linear algebraic equations, expressed in matrix form as,

$$[M]\vec{T} = \vec{q} \quad . \quad (3.1)$$

Direct elimination is always possible but it is time consuming and requires excessive computer core if the dimension of the matrix is large. Methods based on triangular resolution of $[M]$ into a lower and an upper triangular matrix, $[L]$ and $[U]$ respectively, can result in significant savings in computational effort and in storage requirements as compared to other direct methods of solution when $[M]$ is a band matrix. In the particular case when $[M]$ is tri-diagonal the

savings are very great indeed. When partial differential equations in two-dimensional space are approximated by implicit finite difference equations involving function values only at the reference mesh point and at its nearest four neighbor points, the matrix of coefficients of the difference equations has non-zero elements only along five diagonals, viz., the principal diagonal and that on either side of it and two off-diagonal lines. In general, when such a matrix is resolved into $[L]$ and $[U]$, these matrices do not preserve the sparse structure of $[M]$. However, if a matrix which approximates $[M]$ can be found such that it is the product of a lower and of an upper triangular matrix, each of which has non-zero elements on only three diagonal lines corresponding to the non-zero diagonal lines in $[M]$, then it is possible to solve the set of equations by an iterative method and to preserve the benefits arising from the sparseness of the matrix $[M]$.

The expressions presented in Equations (2.15), (2.16), and (2.17), can be simplified in a general form

$$B_{i,j} T_{i,j-1} + D_{i,j} T_{i-1,j} + E_{i,j} T_{i,j} + F_{i,j} T_{i+1,j} + H_{i,j} T_{i,j+1} = q_{i,j}, \quad (3.2)$$

which, expressed in matrix notation, has the form

3.2 Algorithm for Iteration

In order to solve Equation (3.2) iteratively, an inductive algorithm instead of the algorithm described by Stone (1968) will be introduced. In principle, both algorithms have the same outcome, but the former, it seems to us, has a clearer and simpler derivation.

Assume that $T_{i,j}$ can be evaluated from $T_{i,j+1}$ and $T_{i+1,j}$ which are already known. Then let

$$T_{i,j} = e_{i,j} T_{i+1,j} + f_{i,j} T_{i,j+1} + d_{i,j} , \quad (3.4)$$

in which $e_{i,j}$, $f_{i,j}$, and $d_{i,j}$ are subject to determination. Hence by Equation (3.4), $T_{i-1,j}$ and $T_{i,j-1}$ which are unknown can be expressed in the forms

$$T_{i-1,j} = e_{i-1,j} T_{i,j} + f_{i-1,j} T_{i-1,j+1} + d_{i-1,j} , \quad (3.5)$$

and

$$T_{i,j-1} = e_{i,j-1} T_{i+1,j-1} + f_{i,j-1} T_{i,j} + d_{i,j-1} . \quad (3.6)$$

Substitute Equations (3.5) and (3.6) into Equation (3.2), and then we have

$$\begin{aligned} T_{i,j} = & - \frac{F_{i,j}}{D_{i,j} e_{i-1,j} + E_{i,j} + B_{i,j} f_{i,j-1}} T_{i+1,j} - \frac{H_{i,j}}{D_{i,j} e_{i-1,j} + E_{i,j} + B_{i,j} f_{i,j-1}} T_{i,j+1} \\ & + \frac{q_{i,j} - D_{i,j} d_{i-1,j} - B_{i,j} d_{i,j-1}}{D_{i,j} e_{i-1,j} + E_{i,j} + B_{i,j} f_{i,j-1}} - D_{i,j} f_{i-1,j} T_{i-1,j+1} - B_{i,j} e_{i,j-1} T_{i+1,j-1} . \end{aligned} \quad (3.7)$$

Equating the right hand sides of Equations (3.4) and (3.7), we obtain the following relations:

$$- \frac{F_{i,j}}{D_{i,j}e_{i-1,j} + E_{i,j} + B_{i,j}f_{i,j-1}} = e_{i,j} , \quad (3.8)$$

$$- \frac{H_{i,j}}{D_{i,j}e_{i-1,j} + E_{i,j} + B_{i,j}f_{i,j-1}} = f_{i,j} , \quad (3.9)$$

$$\frac{q_{i,j} - D_{i,j}d_{i-1,j} - B_{i,j}d_{i,j-1}}{D_{i,j}e_{i-1,j} + E_{i,j} + B_{i,j}f_{i,j-1}} = d_{i,j} , \quad (3.10)$$

$$D_{i,j}f_{i-1,j} = 0 , \quad (3.11)$$

and

$$B_{i,j}e_{i,j-1} = 0 . \quad (3.12)$$

In the expressions, Equation (3.8) through Equation (3.12), the capitalized elements are all known. If the elements with subscripts $(i-1,j)$ or $(i,j-1)$ are also known from previous calculations, then in the above five relationships we have only three unknowns, $e_{i,j}$, $f_{i,j}$, and $d_{i,j}$. In other words, these three unknowns are indeterminate if all five relationships have to be satisfied; equivalently, we can say that there is no way to resolve the matrix $[M]$ of Equation (3.1) exactly into a product of lower and upper triangular matrices with the same sparse structure as $[M]$, as we previously noted.

In Equation (3.7), the terms containing $T_{i-1,j+1}$ and $T_{i+1,j-1}$ are the source of the trouble. However, if $T_{i-1,j+1}$ and $T_{i+1,j-1}$ can be expressed approximately in terms of $T_{i+1,j}$, or $T_{i,j+1}$, or even $T_{i,j}$ and other known quantities when we evaluate $T_{i,j}$, then we obtain three relationships for three unknowns. Expanding $T_{i-1,j+1}$, $T_{i-1,j}$, and $T_{i,j+1}$ in Taylor series about the grid point (i,j) , we have

$$T_{i-1,j+1} = -T_{i,j} + T_{i,j+1} + T_{i-1,j} + O(\Delta x \Delta z) \quad . \quad (3.13)$$

Similarly,

$$T_{i+1,j-1} = -T_{i,j} + T_{i+1,j} + T_{i,j-1} + O(\Delta x \Delta z) \quad . \quad (3.14)$$

Now it is realized that the right hand sides of the expressions (3.13) and (3.14) have a truncation error $O(\Delta x \Delta z)$ and thus an iterative process is necessary for the solution of Equation (3.3). Therefore, we introduce an iteration parameter α for both expressions (3.13) and (3.14) in the forms

$$T_{i-1,j+1} = \alpha(-T_{i,j} + T_{i,j+1} + T_{i-1,j}) \quad (3.15)$$

and

$$T_{i+1,j-1} = \alpha(-T_{i,j} + T_{i+1,j} + T_{i,j-1}) \quad . \quad (3.16)$$

In principle, two iteration parameters, say α and β may be introduced to the expression Equations (3.13) and (3.14) respectively. However, we use only one iteration parameter α for convenience and for simplifying the numerical experiment.

First consider the expression Equation (3.15). By virtue of the Equation (3.5), Equation (3.15) becomes

$$\begin{aligned} T_{i-1,j+1} = & \alpha(-T_{i,j} + T_{i,j+1}) + \alpha[e_{i-1,j} T_{i,j} \\ & + f_{i-1,j} T_{i-1,j+1} + d_{i-1,j}] \quad , \end{aligned}$$

which gives

$$T_{i-1,j+1} = \alpha \frac{(-1 + e_{i-1,j})T_{i,j} + T_{i,j+1} + d_{i-1,j}}{1 - \alpha f_{i-1,j}} \quad (3.17)$$

Similarly, by use of Equation (3.6), $T_{i+1,j-1}$ is expressed in the form

$$T_{i+1,j-1} = \alpha \frac{(-1 + f_{i,j-1})T_{i,j} + T_{i+1,j} + d_{i,j-1}}{1 - \alpha e_{i,j-1}} \quad (3.18)$$

Finally, substituting Equations (3.17) and (3.18) into Equation (3.7) the result is obtained,

$$\begin{aligned} T_{i,j} = & - \frac{H_{i,j} + \frac{\alpha D_{i,j} f_{i-1,j}}{1 - \alpha f_{i-1,j}}}{E_{i,j} + \frac{D_{i,j} (e_{i-1,j}^{-\alpha f_{i-1,j}})}{1 - \alpha f_{i-1,j}} + \frac{B_{i,j} (f_{i,j-1}^{-\alpha e_{i,j-1}})}{1 - \alpha e_{i,j-1}}} T_{i,j+1} \\ & - \frac{F_{i,j} + \frac{\alpha B_{i,j} e_{i,j-1}}{1 - \alpha e_{i,j-1}}}{E_{i,j} + \frac{D_{i,j} (e_{i-1,j}^{-\alpha f_{i-1,j}})}{1 - \alpha f_{i-1,j}} + \frac{B_{i,j} (f_{i,j-1}^{-\alpha e_{i,j-1}})}{1 - \alpha e_{i,j-1}}} T_{i+1,j} \\ & + \frac{q_{i,j} - \left(\frac{D_{i,j}}{1 - \alpha f_{i-1,j}} \right) d_{i-1,j} - \left(\frac{B_{i,j}}{1 - \alpha e_{i,j-1}} \right) d_{i,j-1}}{E_{i,j} + \frac{D_{i,j} (e_{i-1,j}^{-\alpha f_{i-1,j}})}{1 - \alpha f_{i-1,j}} + \frac{B_{i,j} (f_{i,j-1}^{-\alpha e_{i,j-1}})}{1 - \alpha e_{i,j-1}}} \quad (3.19) \end{aligned}$$

By comparing Equations (3.4) and (3.19), $e_{i,j}$, $f_{i,j}$, and $d_{i,j}$ are obtained inductively as the following expressions,

$$e_{i,j} = - \frac{F_{i,j} + \frac{\alpha B_{i,j} e_{i,j-1}}{1-\alpha e_{i,j-1}}}{E_{i,j} + \frac{D_{i,j} (e_{i-1,j}^{-\alpha f_{i-1,j}})}{1-\alpha f_{i-1,j}} + \frac{B_{i,j} (f_{i,j-1}^{-\alpha e_{i,j-1}})}{1-\alpha e_{i,j-1}}} \quad (3.20)$$

$$f_{i,j} = - \frac{H_{i,j} + \frac{\alpha D_{i,j} f_{i-1,j}}{1-\alpha f_{i-1,j}}}{E_{i,j} + \frac{D_{i,j} (e_{i-1,j}^{-\alpha f_{i-1,j}})}{1-\alpha f_{i-1,j}} + \frac{B_{i,j} (f_{i,j-1}^{-\alpha e_{i,j-1}})}{1-\alpha e_{i,j-1}}} \quad (3.21)$$

and

$$d_{i,j} = \frac{q_{i,j} - \left(\frac{D_{i,j}}{1-\alpha f_{i-1,j}} \right) d_{i-1,j} - \left(\frac{B_{i,j}}{1-\alpha e_{i,j-1}} \right) d_{i,j-1}}{E_{i,j} + \frac{D_{i,j} (e_{i-1,j}^{-\alpha f_{i-1,j}})}{1-\alpha f_{i-1,j}} + \frac{B_{i,j} (f_{i,j-1}^{-\alpha e_{i,j-1}})}{1-\alpha e_{i,j-1}}} \quad (3.22)$$

Now the computational procedure is straightforward and is described as follows:

(1) Since all the capitalized elements and $q_{i,j}$ are known quantities at all grid points, and since Equations (3.20), (3.21), and (3.22) give the expressions of $e_{i,j}$, $f_{i,j}$, and $d_{i,j}$ in terms of these at grid points $(i,j-1)$ and $(i-1,j)$, one can simply evaluate $e_{i,j}$, $f_{i,j}$ and $d_{i,j}$ in the whole field starting from the grid point at the left, lower corner of the field to that at the right, upper corner of the field.

(2) When all the $e_{i,j}$, $f_{i,j}$, and $d_{i,j}$ have been calculated, $T_{i,j}$ can be calculated "explicitly" by Equation (3.19) from the right, upper corner of the field to the left, lower corner provided suitable boundary conditions are given.

It is interesting to note here that the original set of Equations, (3.2), is an implicit one and that, by applying the above stated algorithm, one can solve the equation (approximately) in an "explicit" manner.

Since the right hand sides of Equations (3.15) and (3.16) are only the approximate expressions for $T_{i-1,j+1}$, and $T_{i+1,j-1}$ with truncation error $O(\Delta x \Delta z)$, the calculations from the expressions Equations (3.19) to (3.22) give only a first approximation to the exact solution, and an iterative process is needed to improve the accuracy. Consider Equation (3.1) at the $(m+1)$ iteration.

$$[M] \vec{T}^{(m+1)} = \vec{q} \quad (3.23)$$

which can be rewritten

$$[M] (\vec{T}^{(m+1)} - \vec{T}^{(m)}) = \vec{q} - [M] \vec{T}^{(m)} \quad (3.24)$$

Let $\vec{\delta}^{(m+1)} = \vec{T}^{(m+1)} - \vec{T}^{(m)}$, the changes of T from iteration m to $m+1$, and $\vec{R}^{(m)} = \vec{q} - [M] \vec{T}^{(m)}$, the residuals at iteration m . Therefore, replacing $q_{i,j}$ in Equations (3.22) and (3.19) by $R_{i,j}^{(m)}$,

$$\begin{aligned} R_{i,j}^{(m)} = & q_{i,j} - (B_{i,j} T_{i,j-1}^{(m)} + D_{i,j} T_{i-1,j}^{(m)} + E_{i,j} T_{i,j}^{(m)} + F_{i,j} T_{i+1,j}^{(m)} \\ & + H_{i,j} T_{i,j+1}^{(m)}) \quad (3.25) \end{aligned}$$

and, replacing $T_{i,j}$, $T_{i,j+1}$, and $T_{i+1,j}$ in Equation (3.19) by $\delta_{i,j}^{(m+1)}$, $\delta_{i,j+1}^{(m+1)}$, and $\delta_{i+1,j}^{(m+1)}$, respectively, we obtain the algorithm for the iterative solution of Equation (3.1):

$$\delta_{i,j}^{(m+1)} = e_{i,j} \delta_{i+1,j}^{(m+1)} + f_{i,j} \delta_{i,j+1}^{(m+1)} + d_{i,j} \quad (3.26)$$

where $e_{i,j}$ and $f_{i,j}$ have the same definitions as in Equations (3.20) and (3.21), while $d_{i,j}$ is now given by,

$$d_{i,j} = \frac{R_{i,j}^{(m)} - \left(\frac{D_{i,j}}{1-\alpha f_{i-1,j}} \right) d_{i-1,j} - \left(\frac{B_{i,j}}{1-\alpha e_{i,j-1}} \right) d_{i,j-1}}{E_{i,j} + \frac{D_{i,j}(e_{i-1,j}^{-\alpha f_{i-1,j}})}{1-\alpha f_{i-1,j}} - \frac{B_{i,j}(f_{i,j-1}^{-\alpha e_{i,j-1}})}{1-\alpha e_{i,j-1}}} . \quad (3.27)$$

The iterative process can be continued until the residuals $R_{i,j}^{(m)}$ satisfy a certain criterion, and then $T_{i,j}^{(m+1)}$ is the solution at the corresponding grid points.

3.3 Convergence Rate

The solution expressed in Equation (3.19) together with Equations (3.20), (3.21), and (3.22) is an approximate solution to Equation (3.1).

$$[M] \vec{T} = \vec{q} , \quad (3.1)$$

but is the exact solution to

$$\begin{aligned} & B_{i,j} T_{i,j-1} + D_{i,j} T_{i-1,j} + E_{i,j} T_{i,j} + F_{i,j} T_{i+1,j} + H_{i,j} T_{i,j+1} \\ & - D_{i,j} f_{i-1,j} [T_{i-1,j+1} - \alpha(-T_{i,j} + T_{i,j+1} + T_{i-1,j})] \\ & - B_{i,j} e_{i,j-1} [T_{i+1,j-1} - \alpha(-T_{i,j} + T_{i+1,j} + T_{i,j-1})] = q_{i,j} . \end{aligned} \quad (3.28)$$

The proof can easily be obtained by substituting Equations (3.5) and (3.6) into Equation (3.2) and by the fact that the resultant equation is identical to the result of combining Equations (3.15) and (3.16) with Equation (3.7). The modified Equation (3.2) in matrix form is

$$\left([M] + [N] \right) \vec{T} = \vec{q} \quad . \quad (3.29)$$

Therefore, the convergence rate for the corresponding iterative process for Equation (3.29), i.e.,

$$\left([M] + [N] \right) \vec{T}^{(m+1)} = \left([M] + [N] \right) \vec{T}^{(m)} + \left(\vec{q} - [M] \vec{T}^{(m)} \right) \quad (3.30)$$

can be analyzed.

If \vec{T} is the exact solution to Equation (3.1), then the error of $\vec{T}^{(m)}$ at the m th iteration is defined by

$$\vec{\epsilon}^{(m)} = \vec{T}^{(m)} - \vec{T} \quad . \quad (3.31)$$

Thus, Equation (3.30) can be rewritten into an error equation

$$\begin{aligned} \left([M] + [N] \right) \vec{\epsilon}^{(m+1)} &= \left([M] + [N] \right) \vec{\epsilon}^{(m)} - [M] \vec{\epsilon}^{(m)} \\ &= [N] \vec{\epsilon}^{(m)} \quad , \end{aligned} \quad (3.32)$$

which can also be expressed in the form

$$\begin{aligned} &B_{i,j} \epsilon_{i,j-1}^{(m+1)} + D_{i,j} \epsilon_{i-1,j}^{(m+1)} + E_{i,j} \epsilon_{i,j}^{(m+1)} + F_{i,j} \epsilon_{i+1,j}^{(m+1)} + H_{i,j} \epsilon_{i,j+1}^{(m+1)} \\ &- D_{i,j} f_{i-1,j} [\epsilon_{i-1,j+1}^{(m+1)} - \alpha(-\epsilon_{i,j}^{(m+1)} + \epsilon_{i,j+1}^{(m+1)} + \epsilon_{i-1,j}^{(m+1)})] \\ &- B_{i,j} e_{i,j-1} [\epsilon_{i+1,j-1}^{(m+1)} - \alpha(-\epsilon_{i,j}^{(m+1)} + \epsilon_{i+1,j}^{(m+1)} + \epsilon_{i,j-1}^{(m+1)})] \\ &= -D_{i,j} f_{i-1,j} [\epsilon_{i-1,j+1}^{(m)} - \alpha(-\epsilon_{i,j}^{(m)} + \epsilon_{i,j+1}^{(m)} + \epsilon_{i-1,j}^{(m)})] \\ &- B_{i,j} e_{i,j-1} [\epsilon_{i+1,j-1}^{(m)} - \alpha(-\epsilon_{i,j}^{(m)} + \epsilon_{i+1,j}^{(m)} + \epsilon_{i,j-1}^{(m)})] \quad . \end{aligned} \quad (3.33)$$

In general, the coefficients in Equation (3.33) are not constants but vary from one grid point to another, from one time step to the

next, and from one iteration to the next. However, for indicating how the convergence rate behaves we simply assume

$$B_{i,j} = H_{i,j} \equiv B$$

$$D_{i,j} = F_{i,j} \equiv D$$

and

$$E_{i,j} \equiv -2(B + D) \quad . \quad (3.34)$$

These conditions may satisfy the stream function Equation (2.17) provided $\Delta x = \Delta z$. Further, we assume

$$-D_{i,j} f_{i-1,j} = -B_{i,j} e_{i,j-1} \equiv C \quad . \quad (3.35)$$

The condition expressed by Equation (3.35) applies when i and j become large and grid points are far from boundaries. Hence, using Equations (3.34) and (3.35), with the assumption that the influence of the boundary points is neglected, and by letting

$$\epsilon_{i,j}^{(m)} = \xi^m A_{\gamma,\beta} \exp[\tilde{i} (\gamma\pi i \Delta x + \beta\pi j \Delta z)] \quad (3.36)$$

where $\tilde{i}^2 = -1$, we can obtain the decay factor ξ per iteration for the error component corresponding to γ and β as

$$\xi = \frac{[0.5 C(1-\alpha)K + C\alpha A] + 2CR}{[0.5 C(1-\alpha)K + C\alpha A + S] + 2CR} \quad (3.37)$$

where

$$K = \cos(\gamma\pi\Delta x) \cos(\beta\pi\Delta z) \quad ,$$

$$A = 2 \sin^2 \left(\frac{\gamma\pi\Delta x}{2} \right) \sin^2 \left(\frac{\beta\pi\Delta z}{2} \right) \quad ,$$

$$R = \sin \left(\frac{\gamma\pi\Delta x}{2} \right) \sin \left(\frac{\beta\pi\Delta z}{2} \right) \cos \left(\frac{\gamma\pi\Delta x}{2} \right) \cos \left(\frac{\beta\pi\Delta z}{2} \right)$$

$$S = -D \sin^2 \left(\frac{\gamma\pi\Delta x}{2} \right) - B \sin^2 \left(\frac{\beta\pi\Delta z}{2} \right) .$$

In order to keep $|\xi| < 1$, the iteration parameter α has to be defined. For solving self-adjoint elliptic difference equations, Dupont, Kendall, and Rachford (1968) used an approximate factorization procedure. In their analysis, a Chebyshev sequence of parameters is used to produce a rapid rate of convergence. However, neither Equation (2.15) nor Equation (2.16) is self-adjoint and their method for determining the iteration parameter α is not applicable. As noted by Stone, α has to be less than 1 and the repeated use of any α in the vicinity of 1 results in $|\xi| \geq 1$. In this numerical experiment, both a transient heat conduction difference equation and the difference equations expressed in Equations (2.15), (2.16), and (2.17) have been investigated and we arrived at the same conclusions. Stone suggested that the individual parameters should be geometrically spaced in the manner

$$1 - \alpha_\ell = (1 - \alpha_{\max})^{\ell/(L-1)}, \quad \ell = 0, \dots, L-1,$$

where L is the number of parameters in a cycle and α_{\max} is the maximum iteration parameter. He also suggested a way to compute α_{\max} :

$$1 - \alpha_{\max} = \min \left[\frac{2\Delta x^2}{1 + \frac{KZ\Delta x^2}{KX\Delta z^2}}, \frac{2\Delta z^2}{1 + \frac{KX\Delta z^2}{KZ\Delta x^2}} \right] \quad (3.38)$$

where KX and KZ are the thermal conductivities in the x and z directions in the thermal conduction equation

$$\frac{\partial}{\partial x} \left(KX \frac{\partial T}{\partial x} \right) + \frac{\partial}{\partial z} \left(KZ \frac{\partial T}{\partial z} \right) = - Q \quad , \quad (3.39)$$

in which Q is the strength of local heat source. However, neither Equation (2.11) nor Equation (2.12) can be represented in as simple a form as Equation (3.39), and even if it could be done, α_{\max} calculated according to Equation (3.38) may have a value greater than 1. Hence in this study we simply use the formula

$$1 - \alpha_{\max} = \min \left[\frac{2\Delta x^2}{1 + \frac{\Delta x^2}{\Delta z^2}} , \frac{2\Delta z^2}{1 + \frac{\Delta z^2}{\Delta x^2}} \right] \quad . \quad (3.40)$$

Experience showed that α_{\max} , selected by using Equation (3.40), has no undesirable effects. Stone also indicated a possible way to increase the rate of convergence by use of double alternate iterations. This process can be carried out by iterating from the left-lower corner of the field to its right-upper corner and then from the left-upper corner to the right-lower corner. However, our experience indicated that the double iteration process did not increase the rate of convergence in the problem under study, and, on the contrary, it may sometimes result in a decrease of the convergence rate. For this reason, we apply the process, iterating from the left-lower corner of the field to its right-upper corner. The rate of convergence indicated by Equation (3.37) applies to this process.

Before the iteration method described above was applied to solve Equations (2.15), (2.16) and (2.17), it was tried on a test problem of a flow of homogeneous, viscous fluid with governing equations

$$\frac{\partial \zeta}{\partial t} + \frac{\partial \psi}{\partial z} \frac{\partial \zeta}{\partial x} - \frac{\partial \psi}{\partial x} \frac{\partial \zeta}{\partial z} = \frac{\partial^2 \zeta}{\partial x^2} + \frac{\partial^2 \zeta}{\partial z^2} , \quad (3.41)$$

and

$$\frac{\partial^2 \psi}{\partial x^2} + \frac{\partial^2 \psi}{\partial z^2} = - \zeta , \quad (3.42)$$

and with the boundary conditions

$$\begin{aligned} \zeta = 0 , \psi = 0 \quad \text{on} \quad x = 0.5 , 0 \leq z \leq 0.5; \quad \text{and} \quad 0 \leq x \leq 0.5 , z = 0.5 , \\ \partial \zeta / \partial x = 0 , \quad \partial \psi / \partial x = 0 \quad \text{on} \quad x = 0 , 0 \leq z \leq 0.5 , \end{aligned} \quad (3.43)$$

and

$$\partial \zeta / \partial z , \quad \partial \psi / \partial z = 0 \quad \text{on} \quad 0 \leq x \leq 0.5 , z = 0 .$$

An exact solution of Eqs. (3.41) and (3.42) with boundary conditions (3.43) is given by

$$\psi = \exp(-2\pi^2 t) \cos \pi x \cos \pi z . \quad (3.44)$$

The nonlinear terms in Equation (3.41) vanish identically for the exact solution but, in the computation by means of finite difference approximation, the nonlinear terms do not quite vanish; thus, any instability caused by their presence should be detected.

Since Equation (3.41) is identical to Equation (2.1) when $R_i = 0$ and $R_e = 1$, the forward-backward scheme proposed for high Reynolds number was not used because of the low Reynolds number. Instead, the central difference form is used for $\partial \zeta / \partial x$ and $\partial \zeta / \partial z$. For the numerical calculation, Equation (3.41) is expressed in an implicit finite difference form by

$$\begin{aligned}
& \frac{\zeta_{i,j}^{n+1} - \zeta_{i,j}^n}{\Delta t} + \frac{\psi_{i,j+1}^n - \psi_{i,j-1}^n}{2\Delta z} \times \frac{\zeta_{i+1,j}^{n+1} - \zeta_{i-1,j}^{n+1}}{2\Delta x} \\
& - \frac{\psi_{i+1,j}^n - \psi_{i-1,j}^n}{2\Delta x} \times \frac{\zeta_{i,j+1}^{n+1} - \zeta_{i,j-1}^{n+1}}{2\Delta z} \\
& = \frac{\zeta_{i+1,j}^{n+1} - 2\zeta_{i,j}^{n+1} + \zeta_{i-1,j}^{n+1}}{\Delta x^2} + \frac{\zeta_{i,j+1}^{n+1} - 2\zeta_{i,j}^{n+1} + \zeta_{i,j-1}^{n+1}}{\Delta z^2}
\end{aligned} \tag{3.45}$$

where the superscripts n and $n+1$ denote the time steps $n\Delta t$ and $(n+1)\Delta t$, and Equation (3.42) is expressed in central difference form by

$$\frac{\psi_{i+1,j} - 2\psi_{i,j} + \psi_{i-1,j}}{\Delta x^2} + \frac{\psi_{i,j+1} - 2\psi_{i,j} + \psi_{i,j-1}}{\Delta z^2} = -\zeta_{i,j} \tag{3.46}$$

Figure 4 shows grid points and meshes for the test problem. In the course of calculation, we used

$$\psi = \cos\pi x \cos\pi z$$

and

$$\zeta = \pi^2 \cos\pi x \cos\pi z$$

as the initial conditions which are in fact the exact solution presented in Equation (3.44) when $t = 0$. The calculation field contains 20×20 grid points (including the boundary points); equal mesh size is used for both Δx and Δz , i.e., $\Delta x = \Delta z = 0.5/19$; the time increment Δt is 0.002, which is about twelve times the limit,

$$\Delta t_d \leq \frac{(\Delta x)^2}{4} \tag{3.47}$$

given by stability analysis if Equation (3.41) is expressed in an explicit finite difference form and if it is assumed that the stability criterion is determined by the diffusion terms rather than by the convective terms of Equation (3.41). In fact, it can be shown that the required time increment to satisfy the stability criterion due to the presence of convective terms is

$$\Delta t_c \leq \frac{1}{\frac{|\partial\psi/\partial z|}{\Delta x} + \frac{|\partial\psi/\partial x|}{\Delta z}}, \quad (3.48)$$

which is much greater than Δt_d expressed in Equation (3.47) for our present problem.

As noted in section 3.3, the solution expressed in Equation (3.19) together with Equations (3.20), (3.21), and (3.22) is an approximate solution to Equation (3.1) because of the approximate expressions Equation (3.15) and Equation (3.16) for $T_{i-1,j+1}$ and $T_{i+1,j-1}$. Hence, in order to detect the effects of this approximation on the calculation, we calculate Equation (3.45) once for a given time step and iteratively calculate Equation (3.46) twice. From this process, one can also detect the effects of the presence of nonlinear terms on the calculation. Thus, one can deduce under what conditions Equation (3.45) has to be calculated iteratively in order that the effects due to the nonlinear terms may be taken into account. As a summary of the detailed calculation, the calculated vorticity and stream function and the exact ones at the point $x = 1/19$ and $z = 1/19$ are listed in the following table. The computer used was a CDC 6400.

t	ζ_{exact}	$\zeta_{\text{calc.}}$	ψ_{exact}	$\psi_{\text{calc. 1}}$	$\psi_{\text{calc. 2}}$
0	9.60222368	-----	0.97290862	-----	-----
0.002	9.23052787	9.22078202	0.93524801	0.92459860	0.93348617
0.004	8.87322061	8.85059308	0.89904521	0.88207465	0.89408518
0.006	8.52974445	8.49137856	0.86424380	0.84222221	0.85587786
0.008	8.19956402	8.14333278	0.83078953	0.80469707	0.81901579
0.01	7.88216465	7.80672216	0.79863025	0.76921420	0.78360202
0.012	7.57705158	7.48175327	0.76771583	0.73555790	0.74967254
0.014	7.28374922	7.16853732	0.73799809	0.70357176	0.71722006
0.016	7.00180039	6.86708870	0.70943070	0.67313486	0.68621320
0.018	6.73076560	6.57733479	0.68196914	0.64414754	0.65660749
0.02	6.47022238	6.29912885	0.65557059	0.61652354	0.62835160
0.022	6.21976461	6.03226294	0.63019391	0.59018586	0.60139091

In the table $\psi_{\text{calc. 1}}$ and $\psi_{\text{calc. 2}}$ denote the stream function calculated at the first and second iteration, respectively.

Figure 5 presents the errors in calculated stream function and vorticity compared to their exact values at the corresponding times. At $t = 0.002$, first the vorticity was calculated by Equation (3.45) and then this newly calculated vorticity was used in Equation (3.46) to calculate the stream function iteratively as noted by $\psi_{\text{calc. 1}}$ and $\psi_{\text{calc. 2}}$. These calculations indicate that the result of even the first iteration is quite close to the corresponding exact solution. However, because of the presence of the nonlinear terms the error grows monotonically with time and, thus, it is concluded that for solution of nonlinear difference equations such as Equation (2.15), or Equation (2.16), it is necessary to use an iterative process even when the Reynolds number is small.

Chapter IV

COMPUTATIONAL PROCEDURE

In Chapter III, an iterative method was introduced to solve Equations (2.15), (2.16) and (2.17) expressed in an implicit form. For a better presentation these equations are rewritten in the general form expressed in Equation (3.2):

(i) Temperature field:

$$\begin{aligned}
& - \left(\frac{A_4 w_{i,j}^{n,(m)}}{2\Delta z} + \frac{1}{2P_r R_e \Delta z^2} \right) T_{i,j-1}^{n+1,(m+1)} - \left(\frac{A_2 u_{i,j}^{n,(m)}}{2\Delta x} + \frac{1}{2P_r R_e \Delta x^2} \right) T_{i-1,j}^{n+1,(m+1)} \\
& + \left[\frac{1}{\Delta t} + \frac{u_{i,j}^{n,(m)}}{2\Delta x} (A_2 - A_3) + \frac{w_{i,j}^{n,(m)}}{2\Delta z} (A_4 - A_5) + \frac{1}{P_r R_e} \left(\frac{1}{\Delta x^2} + \frac{1}{\Delta z^2} \right) \right] T_{i,j}^{n+1,(m+1)} \\
& - \left(-\frac{A_3 u_{i,j}^{n,(m)}}{2\Delta x} + \frac{1}{2P_r R_e \Delta x^2} \right) T_{i+1,j}^{n+1,(m+1)} - \left(-\frac{A_5 w_{i,j}^{n,(m)}}{2\Delta z} + \frac{1}{2P_r R_e \Delta z^2} \right) T_{i,j+1}^{n+1,(m+1)} \\
& = \left(\frac{A_4 w_{i,j}^{n,(m)}}{2\Delta z} + \frac{1}{2P_r R_e \Delta z^2} \right) T_{i,j-1}^n + \left(\frac{A_2 u_{i,j}^{n,(m)}}{2\Delta x} + \frac{1}{2P_r R_e \Delta x^2} \right) T_{i-1,j}^n \\
& + \left[\frac{1}{\Delta t} - \frac{u_{i,j}^{n,(m)}}{2\Delta x} (A_2 - A_3) - \frac{w_{i,j}^{n,(m)}}{2\Delta z} (A_4 - A_5) - \frac{1}{P_r R_e} \left(\frac{1}{\Delta x^2} + \frac{1}{\Delta z^2} \right) \right] T_{i,j}^n \\
& + \left(-\frac{A_3 u_{i,j}^{n,(m)}}{2\Delta x} + \frac{1}{2P_r R_e \Delta x^2} \right) T_{i+1,j}^n + \left(-\frac{A_5 w_{i,j}^{n,(m)}}{2\Delta z} + \frac{1}{2P_r R_e \Delta z^2} \right) T_{i,j+1}^n ;
\end{aligned}$$

(4.1)

(ii) Vorticity field:

$$\begin{aligned}
& - \left(\frac{A_4 w_{i,j}^{n,(m)}}{2\Delta z} + \frac{1}{2R_e \Delta z^2} \right) \zeta_{i,j-1}^{n+1,(m+1)} - \left(\frac{A_2 u_{i,j}^{n,(m)}}{2\Delta x} + \frac{1}{2R_e \Delta x^2} \right) \zeta_{i-1,j}^{n+1,(m+1)} \\
& + \left[\frac{1}{\Delta t} + \frac{u_{i,j}^{n,(m)}}{2\Delta x} (A_2 - A_3) + \frac{w_{i,j}^{n,(m)}}{2\Delta z} (A_4 - A_5) + \frac{1}{R_e} \left(\frac{1}{\Delta x^2} + \frac{1}{\Delta z^2} \right) \right] \zeta_{i,j}^{n+1,(m+1)} \\
& - \left(-\frac{A_3 u_{i,j}^{n,(m)}}{2\Delta x} + \frac{1}{2R_e \Delta x^2} \right) \zeta_{i+1,j}^{n+1,(m+1)} - \left(-\frac{A_5 w_{i,j}^{n,(m)}}{2\Delta z} + \frac{1}{2R_e \Delta z^2} \right) \zeta_{i,j+1}^{n+1,(m+1)} \\
& = \left(\frac{A_4 w_{i,j}^{n,(m)}}{2\Delta z} + \frac{1}{2R_e \Delta z^2} \right) \zeta_{i,j-1}^n + \left(\frac{A_2 u_{i,j}^{n,(m)}}{2\Delta x} + \frac{1}{2R_e \Delta x^2} \right) \zeta_{i-1,j}^n \\
& + \left[\frac{1}{\Delta t} - \frac{u_{i,j}^{n,(m)}}{2\Delta x} (A_2 - A_3) - \frac{w_{i,j}^{n,(m)}}{2\Delta z} (A_4 - A_5) - \frac{1}{R_e} \left(\frac{1}{\Delta x^2} + \frac{1}{\Delta z^2} \right) \right] \zeta_{i,j}^n \\
& + \left(-\frac{A_3 u_{i,j}^{n,(m)}}{2\Delta x} + \frac{1}{2R_e \Delta x^2} \right) \zeta_{i+1,j}^n + \left(-\frac{A_5 w_{i,j}^{n,(m)}}{2\Delta z} + \frac{1}{2R_e \Delta z^2} \right) \zeta_{i,j+1}^n \\
& + \frac{R_i}{4} \frac{T_{i+1,j}^{n+1,(m+1)} - T_{i-1,j}^{n+1,(m+1)} + T_{i+1,j}^n - T_{i-1,j}^n}{\Delta x} ; \tag{4.2}
\end{aligned}$$

(iii) Stream function field:

$$\begin{aligned}
& \frac{1}{\Delta z^2} \psi_{i,j-1} + \frac{1}{\Delta x^2} \psi_{i-1,j} - 2 \left(\frac{1}{\Delta x^2} + \frac{1}{\Delta z^2} \right) \psi_{i,j} + \frac{1}{\Delta x^2} \psi_{i+1,j} \\
& + \frac{1}{\Delta z^2} \psi_{i,j+1} = -\zeta_{i,j} . \tag{4.3}
\end{aligned}$$

In the above expressions, the superscripts inside parentheses denote the iteration step within a time step for temperature and vorticity fields.

In the course of computation at time equal to zero, a uniform flow starts impulsively. The stream function field is calculated by letting $\zeta_{i,j} = 0$ in Equation (4.3). Of course, the calculation proceeds iteratively according to the iterative method described in Chapter III. The initial temperature field is assumed to have the same distribution as the initial stream function field. A flow chart for the initial solution is presented in Figure 6. From the initial stream function initial velocities $u_{i,j}$ and $w_{i,j}$ can be calculated to determine the values of A_2 , A_3 , A_4 and A_5 according to the expressions Equation (2.18). Subsequently, the temperature field at the interior points at time Δt can be computed by Equation (4.1) provided the boundary conditions in both inflow and outflow regions, and the velocities of the interior points are kept at the initial values; then, the temperatures on the inflow and outflow boundaries are extrapolated by expressions Equations (2.30c) and (2.31c). The vorticity field at the interior points and on inflow and outflow boundaries at time Δt can be calculated in a similar manner. However, the values of vorticity on the obstacle must be evaluated at time level Δt by Equations (2.21), (2.22) and (2.26) before those at the interior points at time level Δt are calculated. Subsequently with the calculated vorticity at time Δt , the stream function at interior points at time Δt is iteratively calculated by Equation (4.3). Note that the stream function on the inflow and outflow boundaries is that from the $(\ell-1)$ iteration when the ℓ th iteration for interior points is processed and then the values on the inflow and

outflow boundaries at the l th step are extrapolated by Equations (2.30a) and (2.31a) from those at interior points calculated at the l th iteration. The iterative process continues until the convergence criterion

$$\text{Max} |\psi_{i,j}^{(\ell+1)} - \psi_{i,j}^{(\ell)}| < \epsilon, \text{ or } \text{Max} \left| \frac{\psi_{i,j}^{(\ell+1)} - \psi_{i,j}^{(\ell)}}{\psi_{i,j}^{(\ell+1)}} \right| < \delta_1 \text{ is satisfied.}$$

When the Reynolds number is small or, equivalently, when the nonlinear effects are not important, the temperature, vorticity, and stream function at time $2\Delta t$ may be calculated by the process described above. However, usually the boundary conditions and the nonlinear effects are so closely coupled that an iterative process must be used for the temperature and vorticity fields. To carry out the iterative process, we register the temperature and vorticity fields, calculated as described above, as $T_{i,j}^{1,(0)}$ and $\zeta_{i,j}^{1,(0)}$ and denote the associated velocity field by $u_{i,j}^{0,(0)}$, and $w_{i,j}^{0,(0)}$. Subsequently, $T_{i,j}^{1,(m+1)}$ and $\zeta_{i,j}^{1,(m+1)}$ and the associated velocity field $u_{i,j}^{0,(m)}$ and $w_{i,j}^{0,(m)}$ will be calculated until the convergence criteria

$$\text{Max} |T_{i,j}^{1,(m+1)} - T_{i,j}^{1,(m)}| < \epsilon_2, \text{ or } \text{Max} \left| \frac{T_{i,j}^{1,(m+1)} - T_{i,j}^{1,(m)}}{T_{i,j}^{1,(m+1)}} \right| < \delta_2$$

(4.5)

and

$$\text{Max} |\zeta_{i,j}^{1,(m+1)} - \zeta_{i,j}^{1,(m)}| < \epsilon_3, \text{ or } \text{Max} \left| \frac{\zeta_{i,j}^{1,(m+1)} - \zeta_{i,j}^{1,(m)}}{\zeta_{i,j}^{1,(m-1)}} \right| < \delta_3,$$

(4.6)

are satisfied. At this stage the iterative process in this time interval $t = \Delta t$ is complete, and the calculation can be advanced to the next time interval $t = 2\Delta t$. In general, the iterative process can be

applied to the calculation from any time step, say the n th step, to the next time step, say the $n+1$ st step. Figure 6 shows a flow chart describing the iterative process to produce the initial solution. A general flow chart for a transient solution from the n th time step to the $n+1$ st time step is depicted in Figure 7.

Chapter V

RESULTS AND DISCUSSION

Before the numerical calculation starts, the time increment and mesh sizes must be determined from different points of view. In theory, for an implicit scheme there is no restriction on the time increment. However, because of boundary conditions and of the nonlinearity of the equations, an iterative process is always needed for the calculation of vorticity and temperature. If a large time increment is chosen, it is to be expected that, for a given time interval, a large number of iterations will be required. On the other hand, if a small time increment is chosen then, for a given time interval, fewer iterations will be needed but, to reach an asymptotic state, a great number of time steps will be required. There is no way to determine analytically the optimum time increment. The only accessible way is to conduct a numerical experiment and to find out the optimum time increment experimentally. Similarly, the optimum mesh size can also be determined experimentally. Of course, the computer core capacity is the most important restriction when a problem with a large number of grid points is calculated.

Based on experience, we used a small time increment, $\Delta t = 0.03$, for the first calculation starting from $t = 0$, since the flow pattern changes rapidly right after the fluid starts flowing. After that the time increment Δt was increased from one time step to the next by the formula

$$\Delta t = \Delta t + 0.02$$

until the condition $\Delta t > 0.2$ is reached. Thereafter, $\Delta t = 0.2$ or 0.22 , was used. As to the space mesh size, we used $\Delta x = 0.25$ and

$\Delta z = 0.25$. Smaller mesh sizes have been tried, but the limitation in computer storage requires the computation field to be smaller in space and, then, a lot of information beyond the computation field is lost. On the other hand, we tried to use larger mesh size, but the increase in truncation errors was too great and overshadowed the advantage of a larger computation field.

Figures 8 to 14 are the computational results of stream function, vorticity, and temperature at different time steps for a stratified flow with Reynolds number 397, Prandtl number 10, and Richardson number 1.58. The figures are direct prints from microfilm plots generated by CDC 6600 computer. These dimensionless numbers are defined in the expressions (2.10). The horizontal and vertical coordinates are normalized by the height, L , of the vertical fence from the line 56 (Fig. 3); the uniform velocity of the incoming flow is the characteristic velocity; the characteristic temperature difference ΔT is defined by $\Delta T = dT/dz L$ where dT/dz is the temperature gradient far upstream and is a constant in the present study. Figure 8 shows the normalized horizontal and vertical coordinates, the same scale being used for both coordinates.

As noted previously, the fluid starts impulsively as an irrotational flow, and thus, at the early stage of the flow development, the flow pattern deviates little from the irrotational flow pattern. Figure 8 showing the stream function at $t = 0.03$ indicates this situation very clearly from the fact that the streamlines are almost symmetric about the vertical axis of the fence. In Figure 9 the flow pattern at $t = 1.82$ is shown. On the upstream side of the fence, the streamlines are lifted up, while, in the lee side, the streamlines converge to produce a strong downslope current; the constant temperature lines show a

similar pattern. The most interesting thing is the development of vorticity. In the case of homogeneous flow of viscous fluid, vorticity is confined to the region of the boundary layer and it may diffuse toward upstream only when the Reynolds number is very small. However, from Figure 9, we can see that vorticity is not only diffused in the wake region but also exists on the upstream side of fence as a result of vorticity creation by density (or temperature) inhomogeneity.

In Figure 10, lee-waves are being generated and the first wave troughs tilt towards upstream. Figure 11 shows a clearer flow pattern of lee-waves; in particular, the contour lines of vorticity present alternating positive and negative regions indicating the troughs and crests of lee-waves. From Figures 12 to 14, one can see the development of lee-waves approaching an asymptotic state. In Figure 14, at $t = 15.68$, two lee-waves are clearly seen; a third wave, which cannot be observed from the streamline contours, is indicated by the positive region of vorticity in the left hand corner. This numerical calculation can be compared with an experimental result by Pao et al. (1968) for a cylinder of diameter 1.905 cm moving with velocity 2.083 cm/sec in stratified salt water of density gradient $d\rho/dz = 20.15 \times 10^{-4}$, and it will be found that the flow patterns are similar. In the experiment the diameter of cylinder is the characteristic length, while in this numerical calculation, the fence height above the line of symmetry, corresponding to the radius of cylinder in the experiment, serves as the characteristic length. For further comparison, reference may be made to similar flow patterns which have been calculated from the inviscid model (Pao, 1969; Miles, 1968).

Another numerical calculation for $R_e = 5000$, $P_r = 1$, and $R_i = 1.58$ is presented in Figures 15 to 21. This calculation was performed to determine whether the forward and backward scheme proposed for the vorticity and temperature equations of stratified flow can really take care of high Reynolds numbers. The calculation indicates that this scheme gives a stable computation as predicted. In the series of patterns in Figures 15 to 19 with the corresponding time t from 0.03 to 18.42, one can observe a similar flow development to that described in the preceding paragraphs and, of course, lee-waves occur downstream of the obstacle. However, in Figures 20 and 21, undesirable disturbances appear near the inflow boundary. In order to understand these undesirable disturbances, it is necessary to recall the numerical experiments on boundary conditions.

To begin with, we used a set of prescribed stream function, vorticity, and temperature on the inflow boundary. The computational field contains 180×30 grid points with $\Delta x = 0.25$, and $\Delta t = 0.25$, and the vertical fence is located at 120 grid points from the inflow boundary. We found that this kind of undesirable disturbance appeared near the inflow boundary as early as t about 4, and that if the Richardson number was increased, these disturbances might appear even earlier. At first it was thought that these disturbances might have resulted from the particular iterative method. In order to clear this point, a flow of homogeneous fluid over the same obstacle was calculated with the same Reynolds number and boundary conditions. We found that, for this homogeneous flow, there existed no such undesirable disturbance near the upstream boundary and that the computation could be carried on as long as was desired, i.e., the computation scheme was stable and the iterative

method was proven to be very efficient in reducing computational efforts. Hence, it is concluded that these undesirable disturbances are associated with the existence of stratification.

Now, one may ask why these undesirable disturbances exist near the inflow boundary but not near the outflow boundary. Consider a transient flow of stratified fluid passing over an obstacle. The disturbances caused by the presence of this obstacle may propagate towards both upstream and downstream in the form of internal gravity waves. If we have suitable boundary conditions for both inflow and outflow boundaries, these internal gravity waves in the computational field can pass through both boundaries, and as time goes on the asymptotic state can be achieved in the long run. However, if unsuitable boundary conditions are used, the disturbances propagating from the obstacle cannot all pass through the boundaries but may reflect back from the boundaries as artificially introduced disturbances. For this numerical study, the predictor formula expressed in Equation (2.30) and Equation (2.31) was used to extrapolate the disturbances from the interior points to the boundaries. At the outflow boundary, it appears that the outflow can efficiently carry the disturbance away from the computational field. However, at the inflow boundary, any undesirable disturbance which occurs may be brought back into the computational field by the inflow as an artificial disturbance which will finally produce undesirable lee-waves downstream of the inflow boundary. One numerical experiment was made to examine the behavior of these undesirable lee-waves and it was found that they could propagate downstream of the inflow boundary. Clearly, this phenomenon is a kind of computational instability, caused by the interaction of the boundary condition and the flow field although, based on the stability analysis, the computational scheme is stable and convergent.

In short, the effects of boundary conditions on the computation are dependent on the flow phenomena themselves. In the case of homogeneous fluid, the boundary condition at the inflow boundary usually involves no problem since disturbances decay exponentially with distance but, in the case of stratified fluid, the inflow boundary condition becomes crucial since disturbances propagate upstream far from the obstacle and, therefore, this boundary condition must receive careful treatment if meaningful results are to be obtained. This is the reason why, in the problem described herein, the computational region upstream of the obstacle contains more grid points than that downstream. According to experience gained during this numerical experiment, a transformation in coordinates to make the computational field extended towards far upstream and downstream would be helpful. Where a vertical fence as an obstacle is concerned, exponential coordinates and elliptical coordinates may be used so that in the region near the obstacle a fine mesh is available and, in the region far from the fence, a coarse mesh may be used. Thus, not only better accuracy could be obtained but also the flow boundaries of the computational field could be pushed as far away as the computer storage allows. Because of limitation in computing time, these special coordinates have not been tried. However, in principle, their applications should produce no problem in computation if the iterative method introduced in Chapter III is used since, as noted previously, this iterative method is insensitive to the coefficients contained in Equation (3.1) and, in fact, the transformation in coordinates changes only these coefficients but not the basic structure of Equation (3.1).

In order to illustrate how the computation was performed for both flow conditions described above, two tables are listed at the end of

this chapter. Both computations were made for square meshes in Cartesian coordinates. In these tables, the first and second columns indicate the time t at which the computation was made and the time increment Δt , respectively. The third column is the time step being computed measured from the instant when the flow starts impulsively. The fourth and fifth columns denote the iteration numbers for temperature and vorticity and for stream function at a given time step, while the sixth and seventh are the accumulated iteration numbers for the corresponding variables. The first computation listed in Table I has the following convergence criteria for iteration of temperature and vorticity at a given time step $(n+1)$,

$$\text{Max} \left| \frac{\theta_{i,j}^{n+1,(m+1)} - \theta_{i,j}^{n+1,(m)}}{\theta_{i,j}^{n+1,(m+1)}} \right| \leq 0.01 \quad \text{for} \quad |\theta_{i,j}^{n+1,(m+1)}| > 0.1 \quad ,$$

or

$$\text{Max} |\theta_{i,j}^{n+1,(m+1)} - \theta_{i,j}^{n+1,(m)}| \leq 0.001 \quad , \quad \text{for} \quad |\theta_{i,j}^{n+1,(m+1)}| \leq 0.1 \quad ,$$

where $\theta_{i,j} \equiv T_{i,j}$ or $\zeta_{i,j}$

and for stream function using the calculated vorticity at the $(m+1)$ iteration at time step $(n+1)$,

$$\text{Max} \left| \frac{\psi_{i,j}^{(\ell+1)} - \psi_{i,j}^{(\ell)}}{\psi_{i,j}^{(\ell+1)}} \right| \leq 0.01 \quad \text{for} \quad |\psi_{i,j}^{(\ell+1)}| > 0.1 \quad ,$$

or

$$\text{Max} |\psi_{i,j}^{(\ell+1)} - \psi_{i,j}^{(\ell)}| \leq 0.001 \quad \text{for} \quad |\psi_{i,j}^{(\ell+1)}| \leq 0.1 \quad .$$

For the second computation listed in Table II, the convergence criteria are:

(a) $t < 20$

$$\text{Max} \left| \frac{\theta_{i,j}^{n+1,(m+1)} - \theta_{i,j}^{n+1,(m)}}{\theta_{i,j}^{n+1,(m+1)}} \right| \leq 0.01 \quad \text{for} \quad |\theta_{i,j}^{n+1,(m+1)}| > 0.1 ,$$

or

$$\text{Max} |\theta_{i,j}^{n+1,(m+1)} - \theta_{i,j}^{n+1,(m)}| \leq 0.001 \quad \text{for} \quad |\theta_{i,j}^{n+1,(m+1)}| \leq 0.1 ,$$

where $\theta_{i,j} \equiv T_{i,j}$ or $\zeta_{i,j}$,

and

$$\text{Max} \left| \frac{\psi_{i,j}^{(\ell+1)} - \psi_{i,j}^{(\ell)}}{\psi_{i,j}^{(\ell+1)}} \right| \leq 0.01 \quad \text{for} \quad |\psi_{i,j}^{(\ell+1)}| > 0.1 ,$$

or

$$\text{Max} |\psi_{i,j}^{(\ell+1)} - \psi_{i,j}^{(\ell)}| \leq 0.001 \quad \text{for} \quad |\psi_{i,j}^{(\ell+1)}| \leq 0.1 .$$

(b) $t \geq 20$

$$\text{Max} \left| \frac{\theta_{i,j}^{n+1,(m+1)} - \theta_{i,j}^{n+1,(m)}}{\theta_{i,j}^{n+1,(m+1)}} \right| \leq 0.001 , \quad \text{for} \quad |\theta_{i,j}^{n+1,(m+1)}| > 0.1$$

or

$$\text{Max} |\theta_{i,j}^{n+1,(m+1)} - \theta_{i,j}^{n+1,(m)}| \leq 0.0001 \quad \text{for} \quad |\theta_{i,j}^{n+1,(m+1)}| \leq 0.1 ,$$

where $\theta_{i,j} \equiv T_{i,j}$ or $\zeta_{i,j}$,

and

$$\text{Max} \left| \frac{\psi_{i,j}^{(\ell+1)} - \psi_{i,j}^{(\ell)}}{\psi_{i,j}^{(\ell+1)}} \right| \leq 0.001 \quad \text{for} \quad |\psi_{i,j}^{(\ell+1)}| > 0.1$$

or

$$\text{Max} |\psi_{i,j}^{(\ell+1)} - \psi_{i,j}^{(\ell)}| \leq 0.0001 \quad \text{for} \quad |\psi_{i,j}^{(\ell+1)}| \leq 0.1 \quad .$$

From columns 4 and 5 of Tables I and II, it can be seen that when the computation starts, a number of iterations is needed since, in the early stages, the flow is highly time-dependent. As the computation goes through the middle course, the iteration numbers are as low as 2. Indeed this situation clearly indicates that the iterative method introduced in Chapter III is really a good one. It is noted that in Pearsons work (1965), a smoothing parameter was introduced for both the boundary and interior points to reduce the computational efforts by decreasing iteration numbers for vorticity calculation at a given time step; it seems to us that the iteration parameter α for the present iteration method may have this effect. For the first computation, 79 time steps were calculated and 30 minutes of CDC 6600 computer time were spent; on the average, each time step took 25 seconds approximately. One thing must be noted about the last row of the Table II which shows that at time $t = 23.46$ a great number of iterations was made for temperature and vorticity as well as for stream function. Comparison of these values with the corresponding ones at $t = 20.52$ indicates that the great number of iterations is not due to the smaller residuals used for convergence criteria when $t \geq 20$. In fact, one may relate this situation to the computational instability caused by the unsuitable boundary conditions as described above. In other words, if this difficulty

particularly involved in the numerical calculation of stratified flows can be removed by some special coordinates, the iterative method is indeed a good one for the numerical calculation of general problems in geophysical fluid mechanics.

TABLE I

t	Δt	Time Step n	Iteration Number for Temperature, T , and Vorticity, ζ	Iteration Number for Stream Function, ψ	Accumulated Iteration Number for Temperature, T , and Vorticity, ζ	Accumulated Iteration Number for Stream Function, ψ
0.03	0.03	1	5	14	5	14
1.82	0.2	13	4	5	53	81
4.76	0.2	27	2	3	95	137
8.76	0.22	46	2	2	133	176
9.80	0.2	51	2	2	143	186
12.74	0.2	65	2	2	171	214
15.68	0.2	79	7	9	213	272

$R_e = 397$, $P_r = 10$, $R_i = 1.58$, $\Delta x = 0.25$, $\Delta z = 0.25$

Grid Points = 180 x 30, Computer Time (CDC 6600) = 30 min., Total core used 51,100 decimal.

TABLE II

t	Δt	Time Step n	Iteration Number for Temperature, T , and Vorticity, ζ	Iteration Number for Stream Function, ψ	Accumulated Iteration Number for Temperature, T , and Vorticity, ζ	Accumulated Iteration Number for Stream Function, ψ
0.03	0.03	1	5	14	5	14
2.88	0.22	18	4	5	73	105
8.34	0.22	44	2	2	131	174
13.38	0.22	68	2	2	179	222
18.42	0.22	92	2	2	227	270
20.52	0.22	102	5	9	256	315
23.46	0.22	116	47	226	557	849

$R_e = 5000.$, $P_r = 1.$, $R_i = 1.58$, $\Delta x = 0.25$, $\Delta z = 0.25$,

Computer Time (CDC 6600) = 60 min., Grid Points = 180 x 30, Total core used 51,100 decimal.

BIBLIOGRAPHY

BIBLIOGRAPHY

1. Dupont, T., Kendall, R. P., and Rachford, H. H. Jr., 1968, "An Approximate Factorization Procedure for Solving Self-Adjoint Elliptic Difference Equations," *J. Num. Anal. SIAM.*, Vol. 5, No. 3, pp. 559-573.
2. Foldvik, A. and Wurtele, M. G., 1967, "The Computation of the Transient Gravity Waves," *Geophys. J. R. Astr. Soc.*, Vol. 13, pp. 161-185
3. Fromm, J. E., and Harlow, F. H., 1963, "Numerical Solutions of the Problem of Vortex Street Development," *Phys. Fluids*, Vol. 6, No. 7, p. 975.
4. Holmboe, J. and Klieforth, H., 1957, "Investigations of Mountain Lee-Waves and the Air Flow over the Sierra Nevada," Dept. Meteor., University of California, Los Angeles.
5. Hovermale, J. B., 1965, "A Nonlinear Treatment of the Problem of Air Flow over Mountains," Doctoral dissertation, Dept. Meteor., Pennsylvania State University.
6. Hung, T. K., 1966, "Laminar Flow in Conduit Expansions," Doctoral dissertation, Dept. Mech. and Hydraulics, University of Iowa.
7. Lin, J. T. and Binder, G. J., 1967, "Simulation of Mountain Lee-Waves in a Wind Tunnel," *Fluid Mech. Prog., Fluid Dynamics and Diffusion Lab.*, Colorado State University, Fort Collins.
8. Long, R. R., 1953, 1955, "Some Aspects of the Flow of Stratified Fluids, I, A Theoretical Investigation," *Tellus*, Vol. 5, pp. 42-58, "III, Continuous Density Gradients," *Tellus*, Vol. 7, pp. 341-357.
9. Long, R. R., 1959, "A Laboratory Model of Air Flow Over the Sierra Nevada Mountains," *The Rossby Memorial Vol.*, pp. 372-380.
10. Lyra, G., 1943, "Theorie der Stationären Leewellmströmung in Freier Atmosphäre," *Zeit. f. Angew. Math. Mech.* Vol. 23, pp. 1-28.
11. Miles, J. W., 1968, 1969, "Lee Waves in a Stratified Flow, Pt. 1, Thin Barrier," *J. Fluid Mech.*, Vol. 32, pp. 549-567; "Pt. 2, Semicircular Obstacle," *J. Fluid Mech.*, Vol. 33, pp. 803-814.
12. Pao, Y. H., Callahan, M. E. and Timm, G. K., 1968, "Vortex Streets in Stably Stratified Fluids," *Boeing Sci. Res. Lab.*, Document D1-82-0736.
13. Pao, Y. H., 1969, "Inviscid Flows of Stably Stratified Fluids over Barriers," *Quart. J. Roy. Meteor. Soc.*, Vol. 95, No. 403, pp. 104-115.

14. Pao, Y. H., and Daugherty, R. J., 1969, "Time-Dependent Viscous Incompressible Flow Past a Finite Flat Plate," Boeing Sci. Res. Lab., Document D1-82-0822.
15. Peaceman, D. W., and Rachford, H. H. Jr., 1955, "The Numerical Solution of Parabolic and Elliptic Differential Equations," J. Soc. Indust. Appl. Math., Vol. 3, pp. 28-41.
16. Pearson, C. E., 1965, "A Computational Method for Viscous Flow Problems," J. Fluid Mech., Vol. 21, Pt. 4, pp. 611-622.
17. Queney, P., 1947, "Theory of Perturbations in Stratified Currents with Application to Air Flow over Mountain Barriers," Dept. Meteor., University of Chicago, Misc. Rept. No. 23.
18. Richtmyer, R. D., and Morton, K. W., 1967, "Difference Method for Initial-Value Problems," Wiley and Sons (2nd Ed.).
19. Scorer, R. S., 1949, "Theory of Waves in the Lee of Mountains," Quart. J. Roy. Meteor. Soc., Vol. 75, pp. 41-56.
20. Stone, H. L., 1968, "Iterative Solution of Implicit Approximations of Multi-dimensional Partial Differential Equations," J. Num. Anal. SIAM, Vol. 5, pp. 530-558.
21. Thoman, D. C., and Szewczyk, A. A., 1966, "Numerical Solutions of Time-Dependent Two-Dimensional Flow of a Viscous, Incompressible Fluid over Stationary and Rotating Cylinders," Dept. Mech. Engr., Univ. Notre Dame, Tech. Rept. 66-14.
22. Yih, C. S., 1960, "Exact Solutions for Steady Two-Dimensional Flow of a Stratified Fluid," J. Fluid Mech., Vol. 9, pp. 161-174.

FIGURES

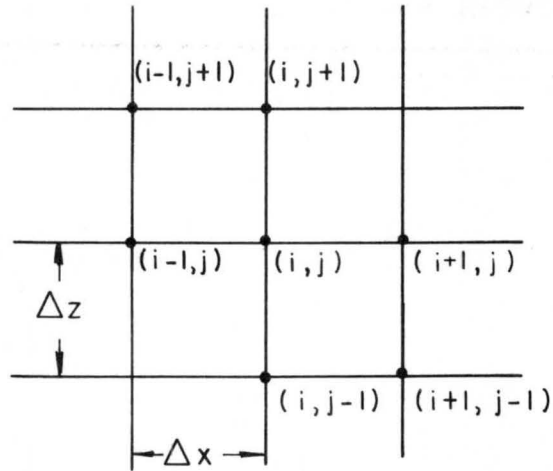


Figure 1 Sketch of Grid Points, and Mesh Sizes

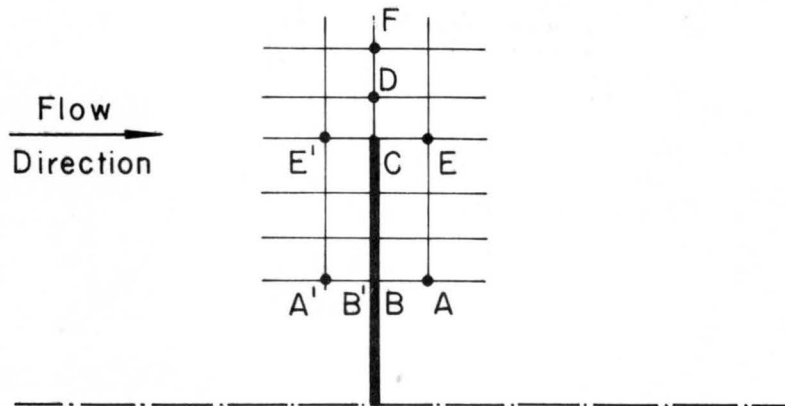


Figure 2 Sketch of Mesh in Vicinity of the Vertical Fence

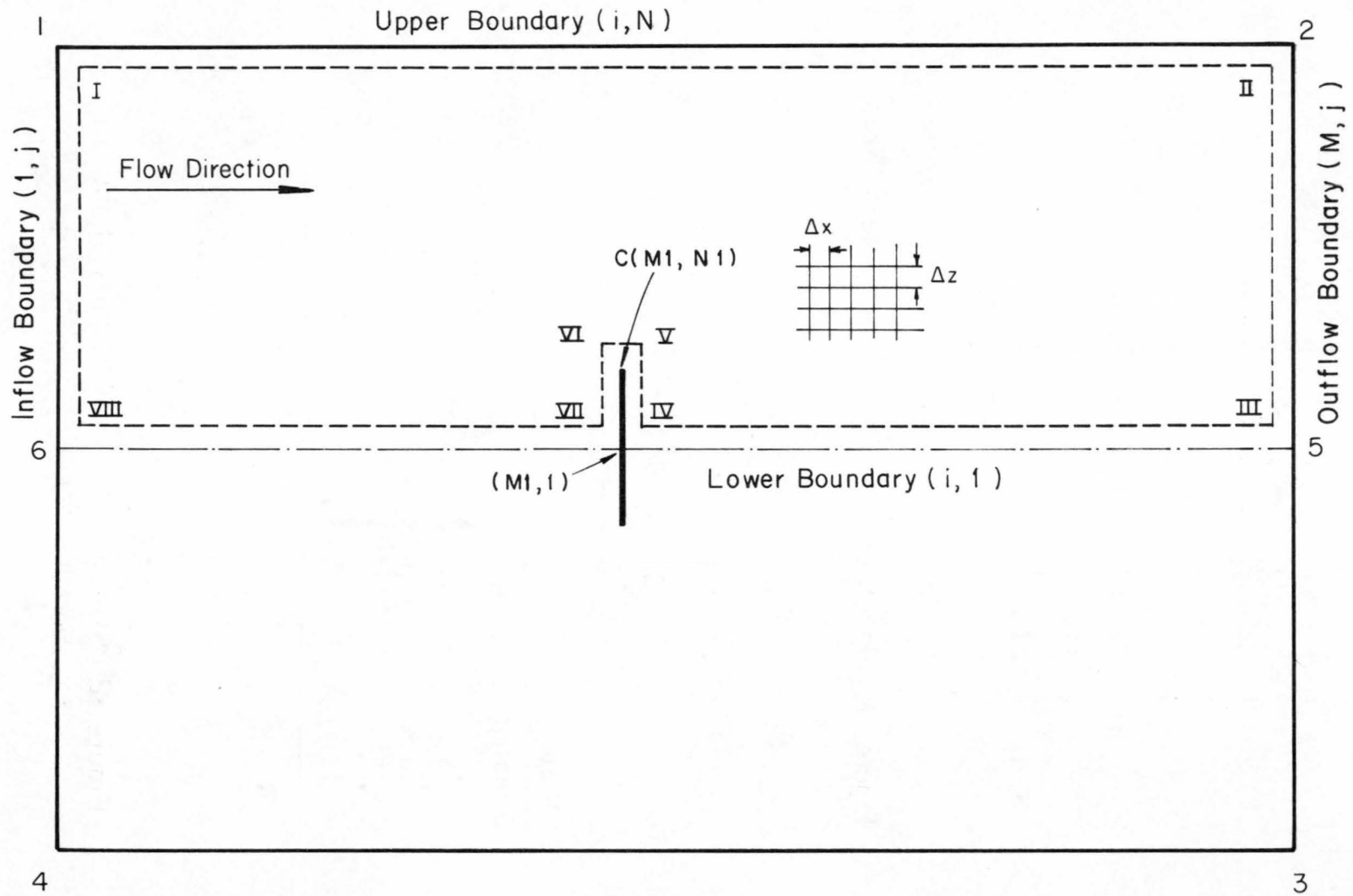


Figure 3 Sketch of Interior Field and Boundaries of Stratified Flow Problem

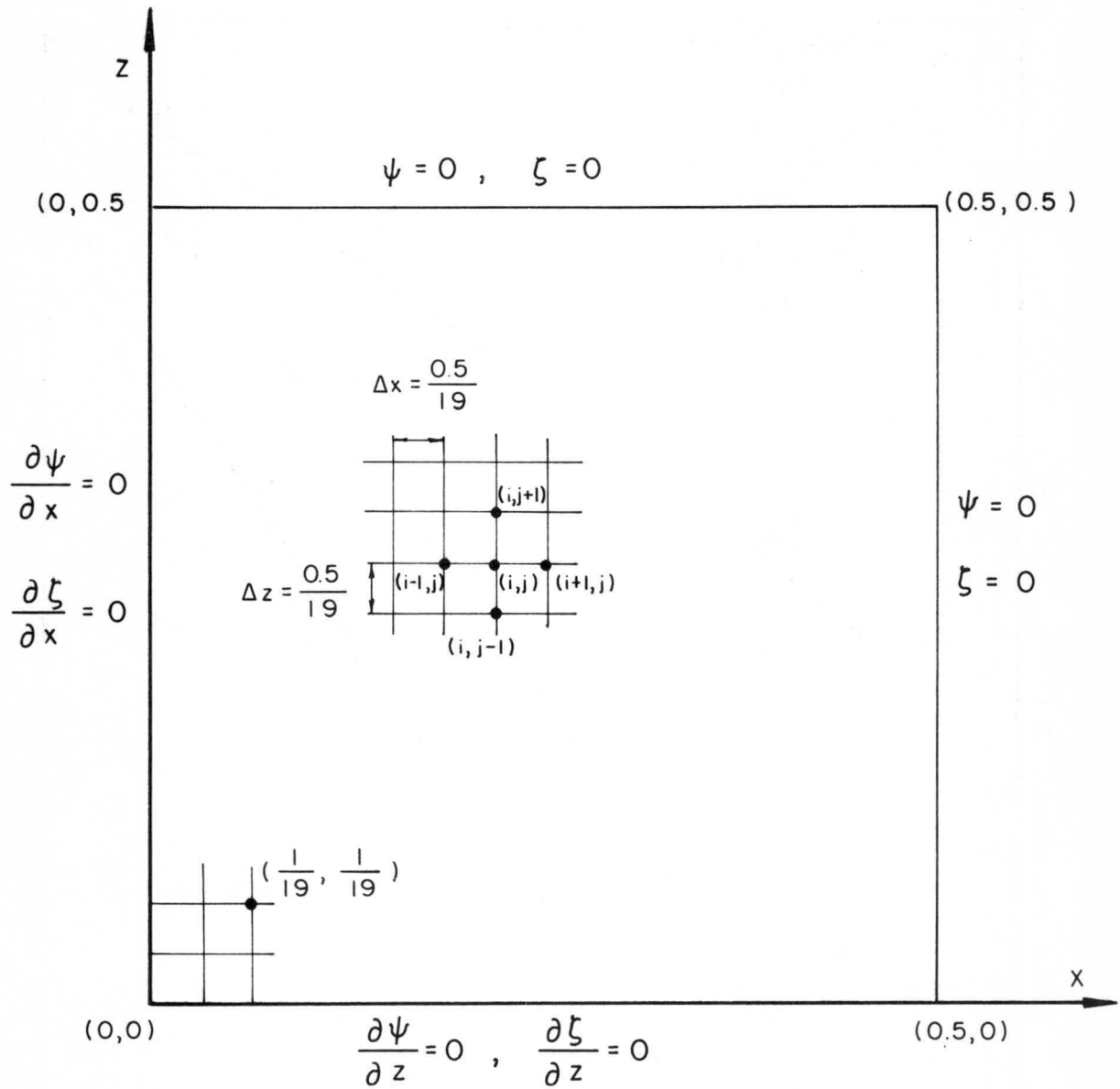


Figure 4 Sketch of Interior Field and Boundary of the Test Problem

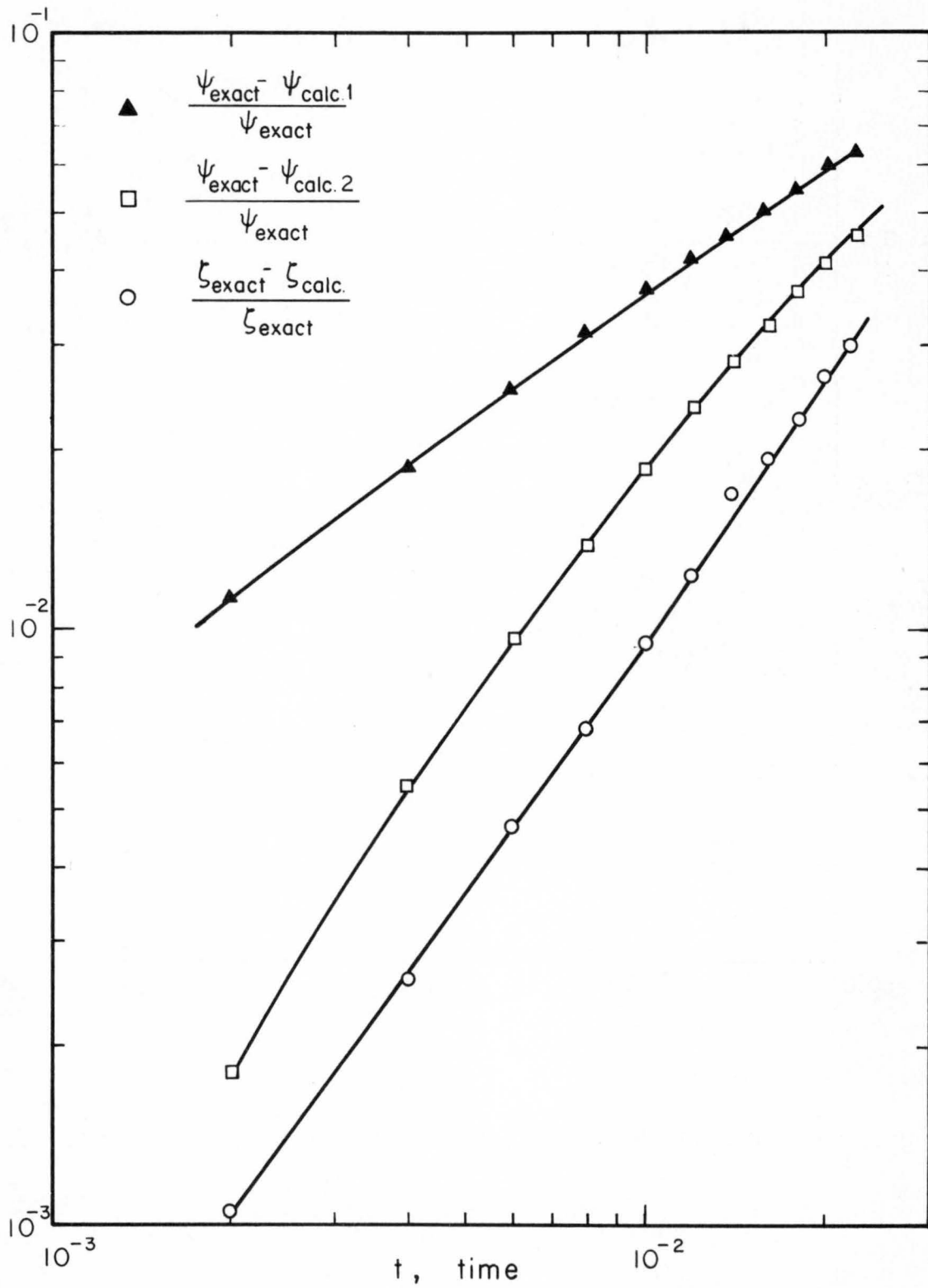


Figure 5 Error Propagation for the Test Problem

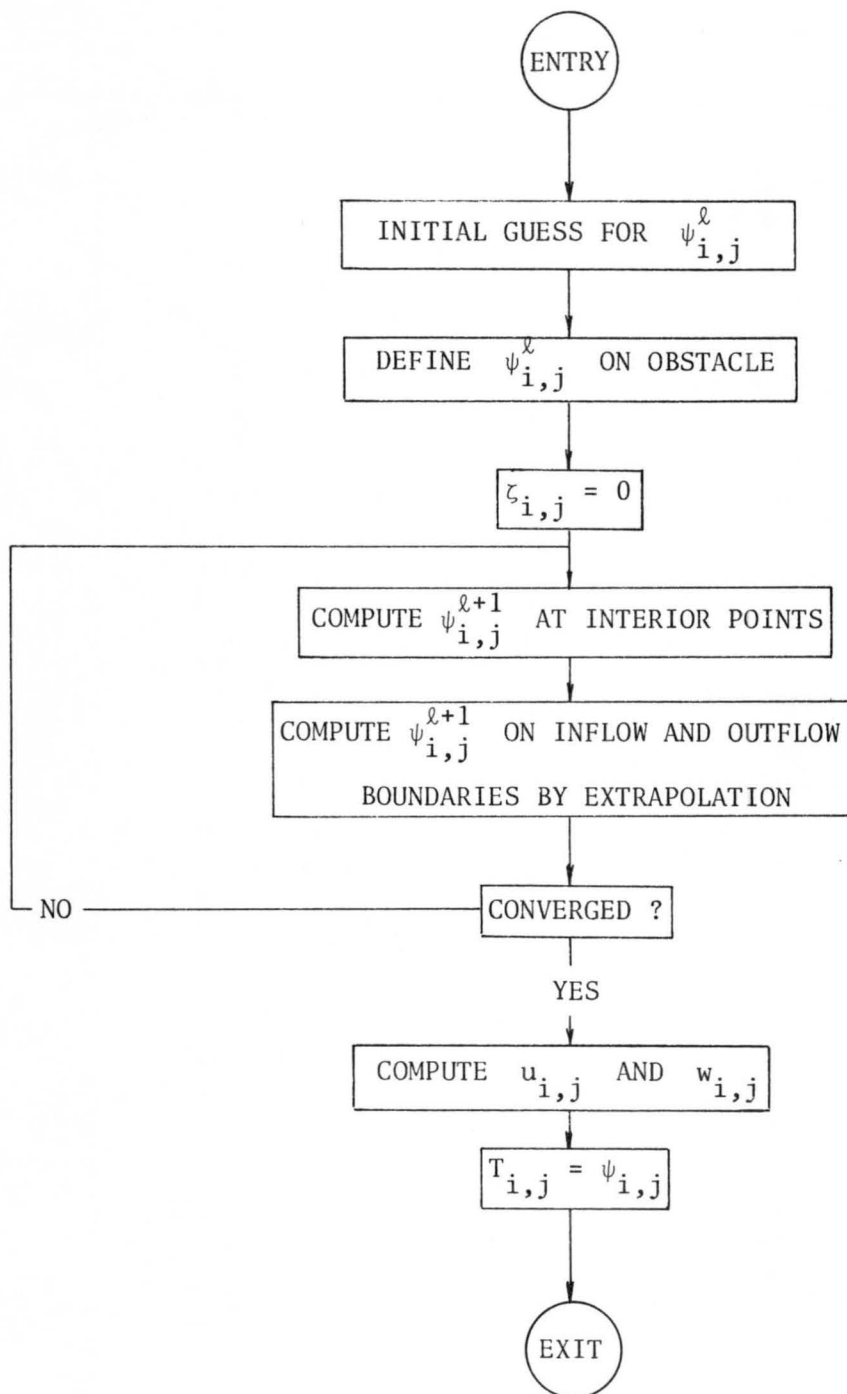


Fig. 6. Flow Chart for Initial Solution

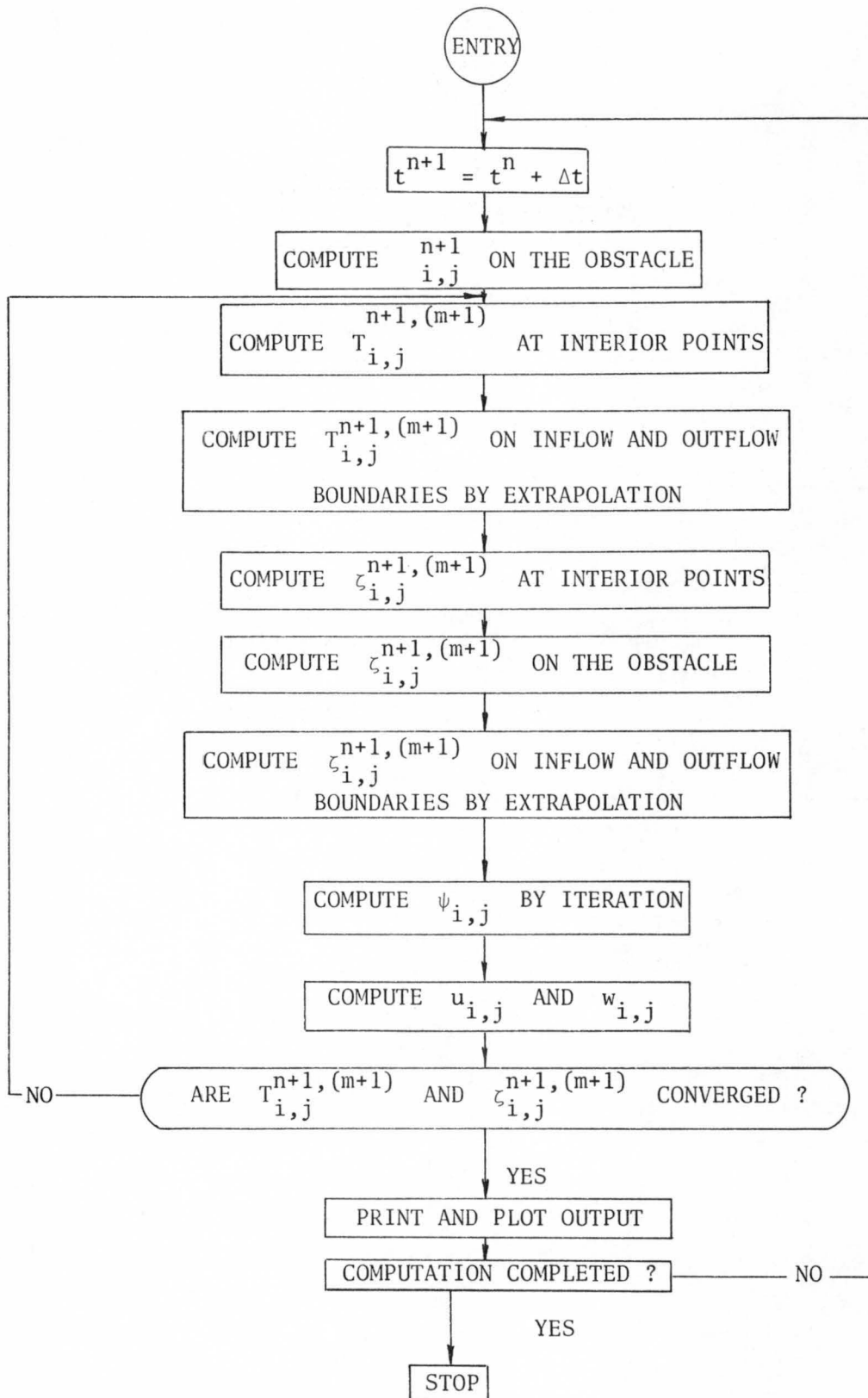
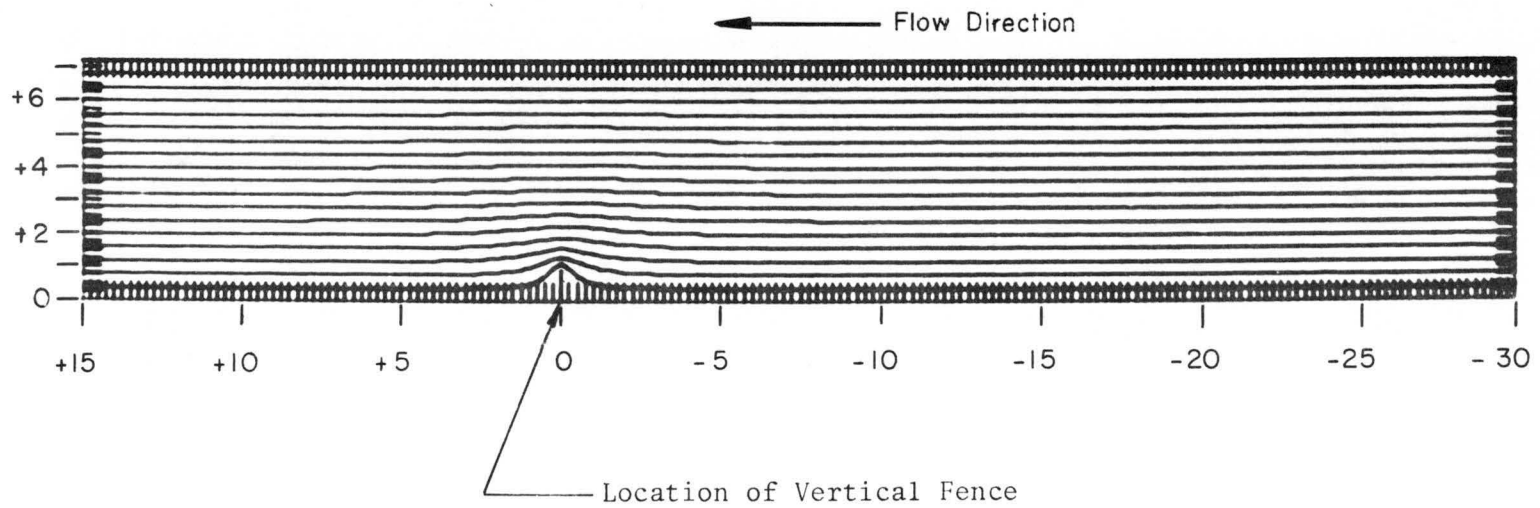


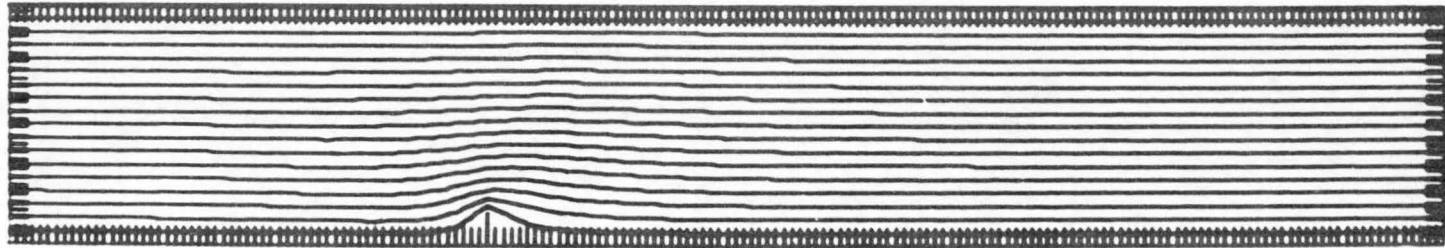
Fig. 7. Flow Chart for Transient Solution



Contour From 0. To 7.200E+00 Contour Interval of 4.00E-01
 Scaled By 1E+02 Pt(3.3) = 5.000E-01

Fig. 8. Stream Function At $t = 0.03$, $Re = 397$, $Pr = 10$, $Ri = 1.58$
 $\Delta X = 0.25$, $\Delta Z = 0.25$, $\Delta t = 0.03$, grid points (180 x 30)

Stream
Function



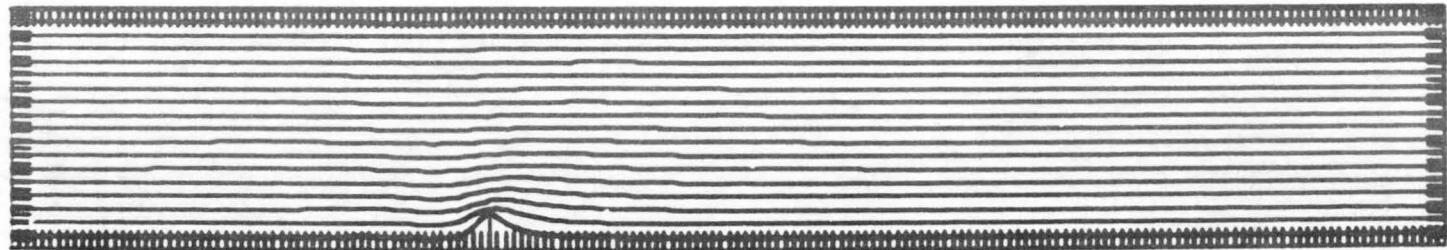
Contour From 0. To $7.200E+00$ Contour interval of $4.000E-01$
Scaled by $1E+02$ Pt(3.3) = $5.000E-01$

Vorticity



Contour From $-5.400E+00$ to $3.000E-01$ Contour Interval of $3.000E-01$
Scaled By $1E+02$ Pt(3.3) = $-3.643E-07$

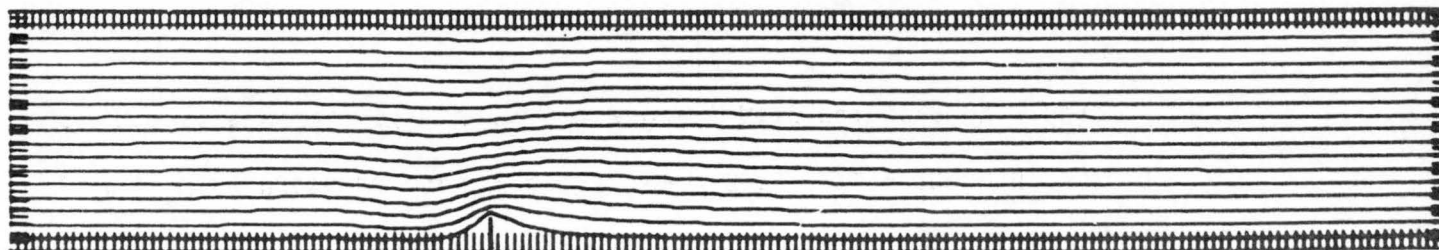
Temperature



Contour From 0. To $7.200E+00$ Contour Interval of $4.000E-01$
Scaled by $1E+02$ Pt(3.3) = $5.000E-01$

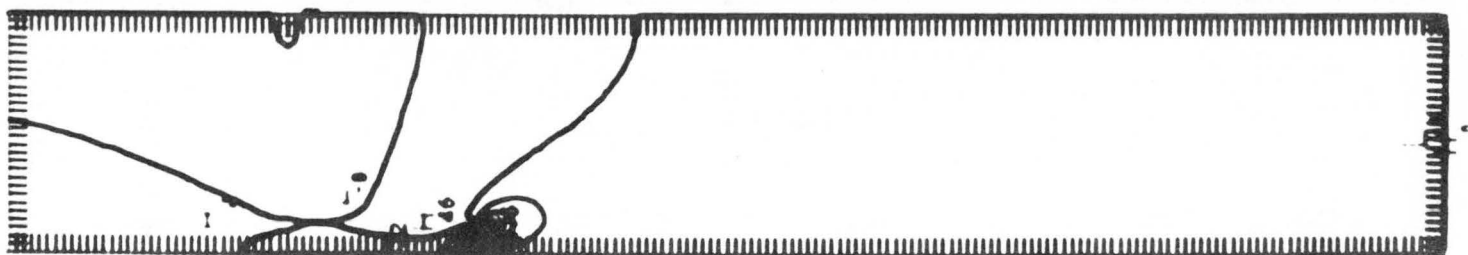
Fig. 9. Flow Patterns At $t = 1.82$, $Re = 397$, $Pr = 10$, $Ri = 1.58$,
 $\Delta X = 0.25$, $\Delta Z = 0.25$, $\Delta t = 0.20$, grid point (180 x 30)

Stream
Function



Contour From 0. To 7.200E+00 Contour Interval of 4.000E-01
Scaled by 1E+02 Pt(3.3) = 5.000E-01

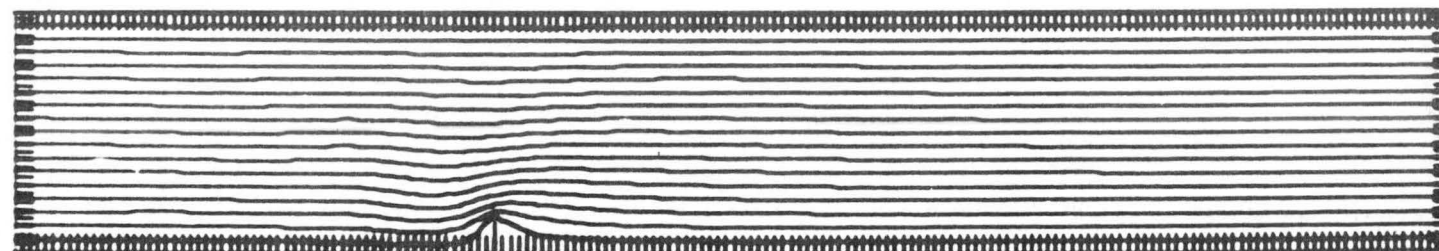
Vorticity



Contour From -4.500E+00 to 3.000E-01 Contour Interval of 3.000E-01
Scaled By 1E+02 Pt(3.3) = -1.792E-05

67

Temperature

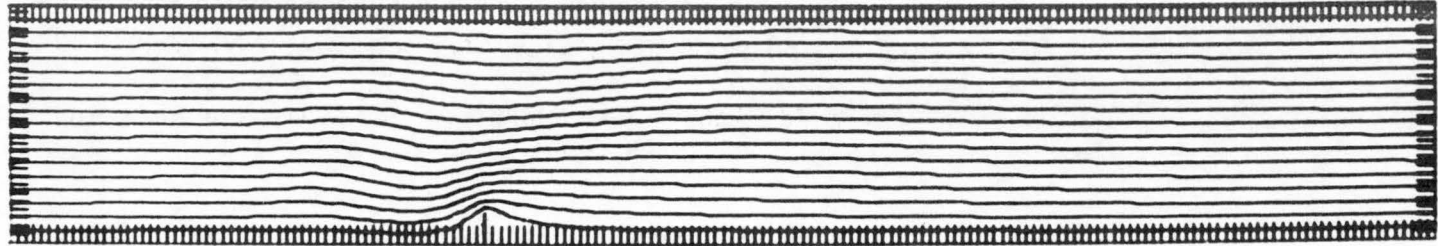


Contour From 0. To 7.200E+00 Contour Interval of 4.000E-01
Scaled By 1E+02 Pt (3.3) = 5.000E-01

Fig. 10. Flow Patterns At $t = 4.76$, $Re = 397$, $Pr = 10$, $Ri = 1.58$,

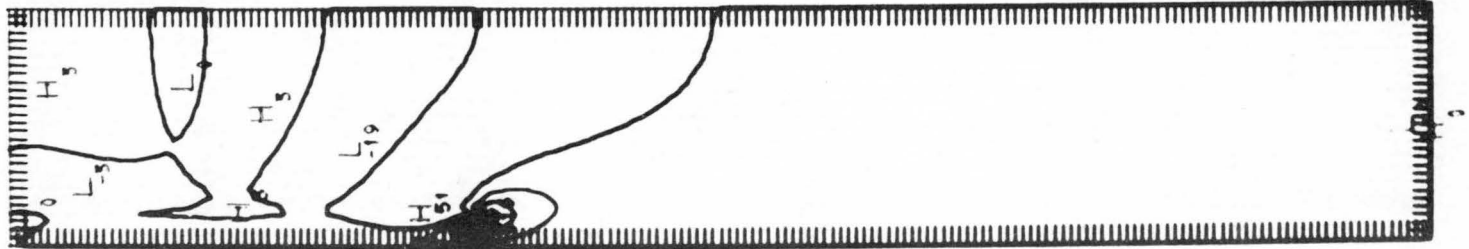
$\Delta X = 0.25$, $\Delta Z = 0.25$, $\Delta t = 0.20$, grid points (180 x 30)

Stream
Function



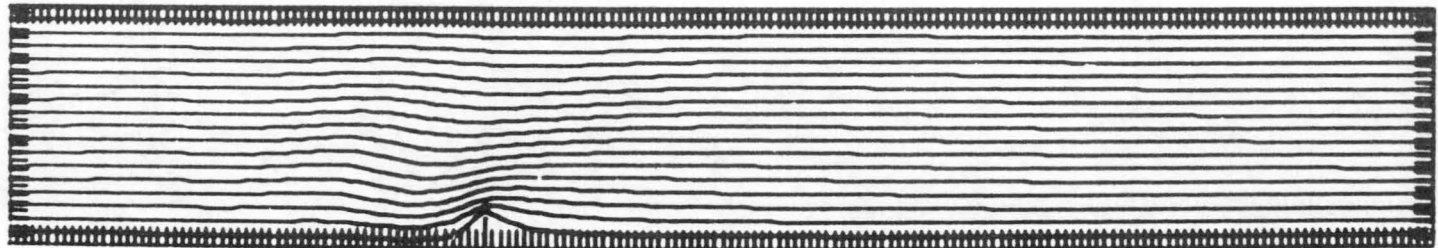
Contour From 0. To 7.200E+00 Contour Interval of 4.000E-01
Scaled By 1E+02 Pt(3.3) = 4.996E-01

Vorticity



Contour From -5.100E+00 To 3.000E-01 Contour Interval of 3.000E-01
Scaled By 1E+02 Pt(3.3) = -3.239E-04

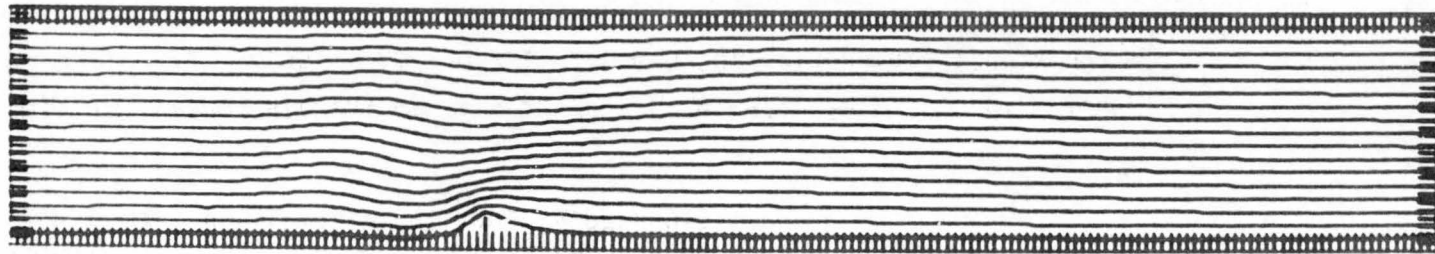
Temperature



Contour From 0. To 7.200E+00 Contour Interval of 4.000E-01
Scaled by 1E+02 Pt(3.3) = 4.997E-01

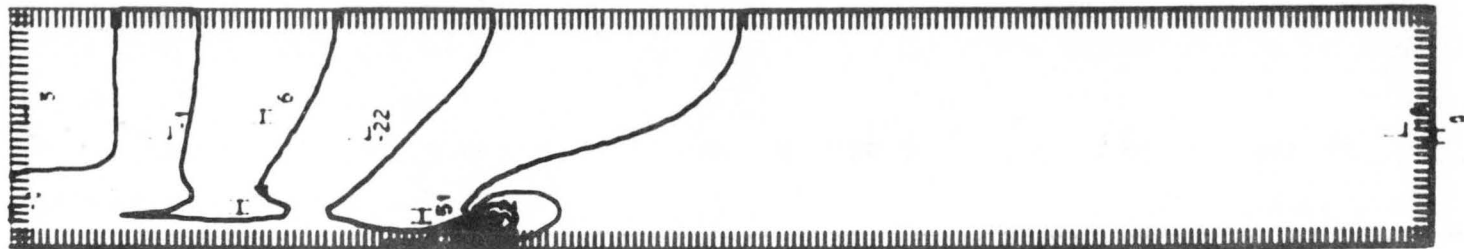
Fig. 11. Flow Patterns At $t = 20.52$, $Re = 397$, $Pr = 10$, $Ri = 1.58$,
 $\Delta X = 0.25$, $\Delta Z = 0.25$, $\Delta t = 0.22$, grid points (180 x 30)

Stream
Function



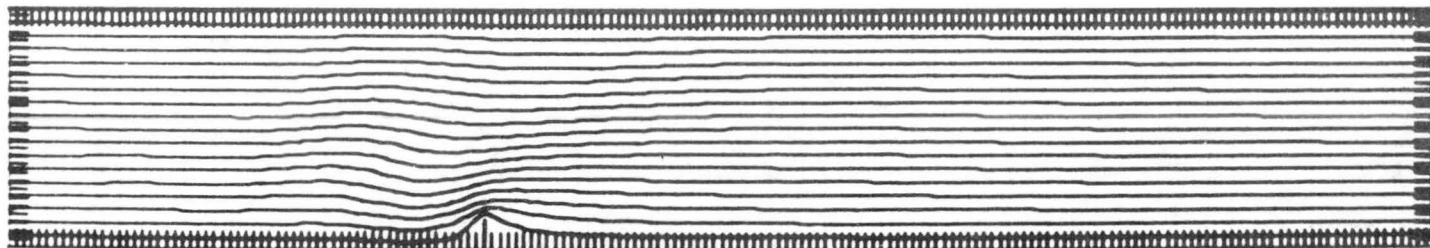
Contour From 0. To 7.200E+00 Contour Interval of 4.000E-01
Scaled By 1E+02 Pt(3.3) = 4.993E-01

Vorticity



Contour From -5.100E+00 To 3.000E-01 Contour Interval of 3.000E-01
Scaled by 1E+02 Pt(3.3) = -6.010E-04

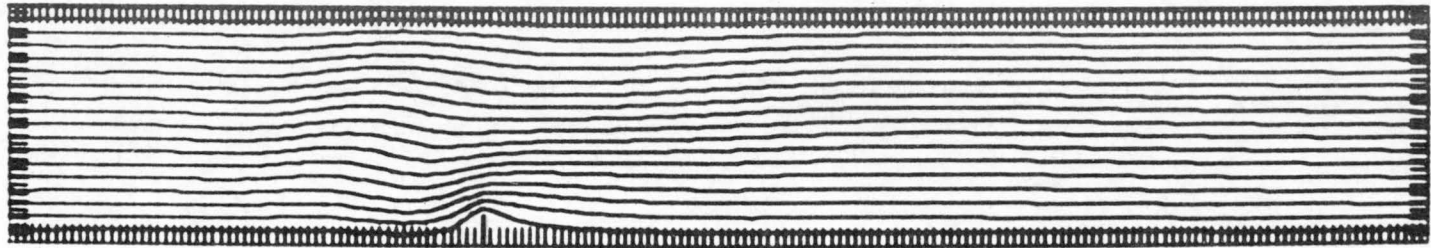
Temperature



Contour From 0. To 7.200E+00 Contour Interval of 4.000E-01
Scaled By 1E+02 Pt(3.3) = 4.995E-01

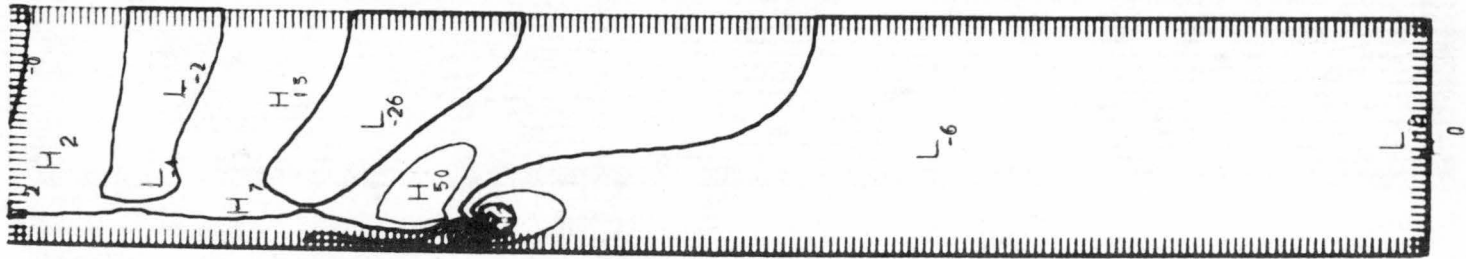
Fig. 12. Flow Patterns At $t = 9.8$, $Re = 397$, $Pr = 10$, $Ri = 1.58$,
 $\Delta X = 0.25$, $\Delta Z = 0.25$, $\Delta t = 0.20$, grid points (180 x 30)

Stream
Function



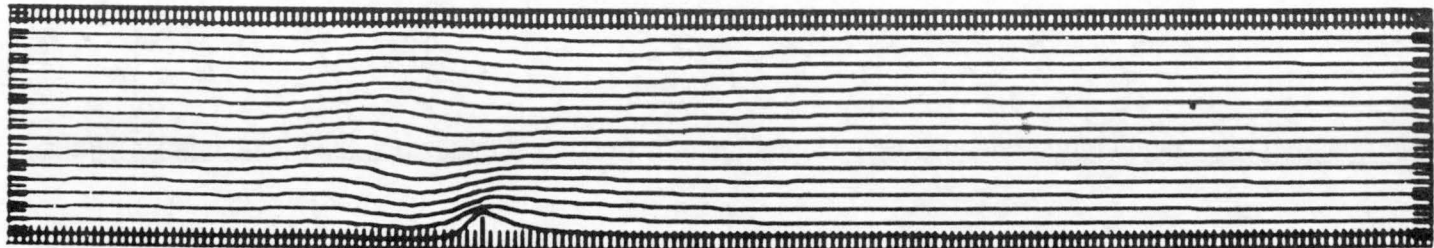
Contour From 0. To 7.200E+00 Contour Interval of 4.000E-01
Scaled By 1E+02 Pt(3.3) = 4.972E-01

Vorticity



Contour From -4.800E+00 to 3.000E-01 Contour Interval of 3.000E-01
Scaled by 1E+02 Pt (3.3) = -2.656E-03

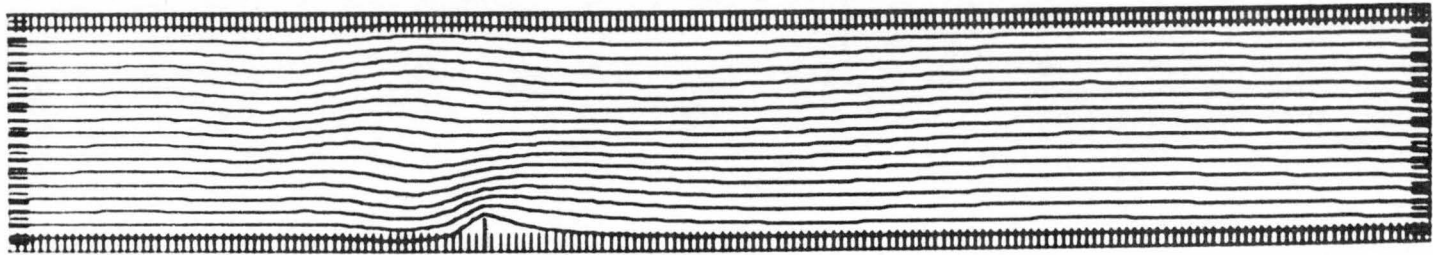
Temperature



Contour From 0. To 7.200E+00 Contour Interval of 4.000E-01
Scaled By 1E+02 Pt (3.3) = 4.979E-01

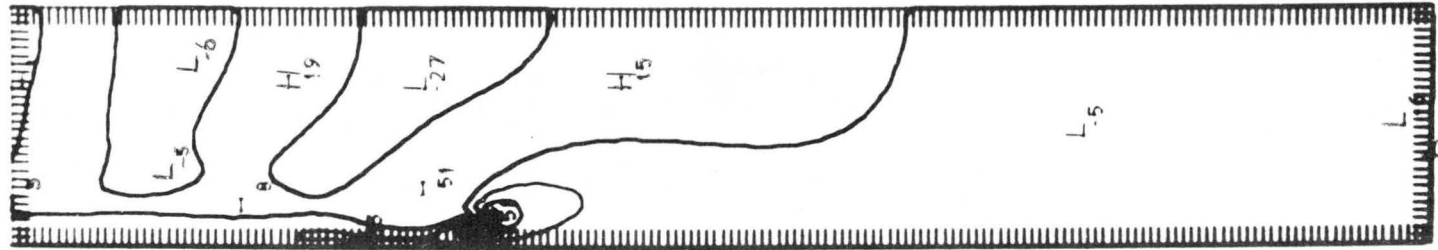
Fig. 13. Flow Patterns At $t = 12.74$, $Re = 397$, $Pr = 10$, $Ri = 1.58$,
 $\Delta X = 0.25$, $\Delta Z = 0.25$, $\Delta t = 0.20$, grid points (180 x 30)

Stream
Function



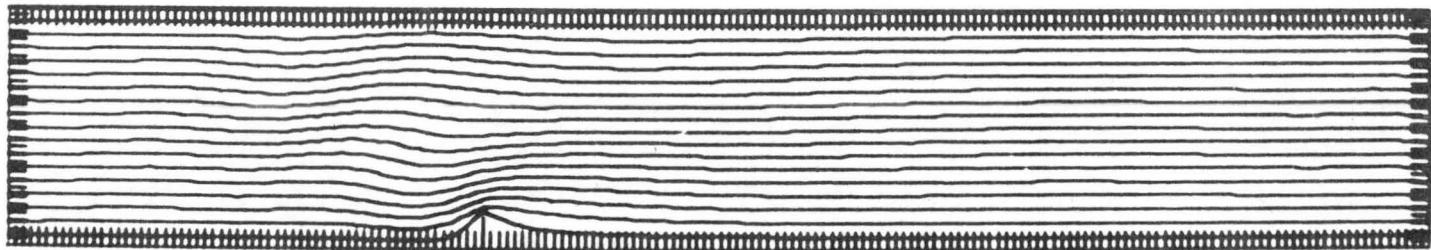
Contour From 0. To 7.200E+00 Contour Interval of 4.000E-01
Scaled By 1E+02 Pt(3.3) = 4.914E-01

Vorticity



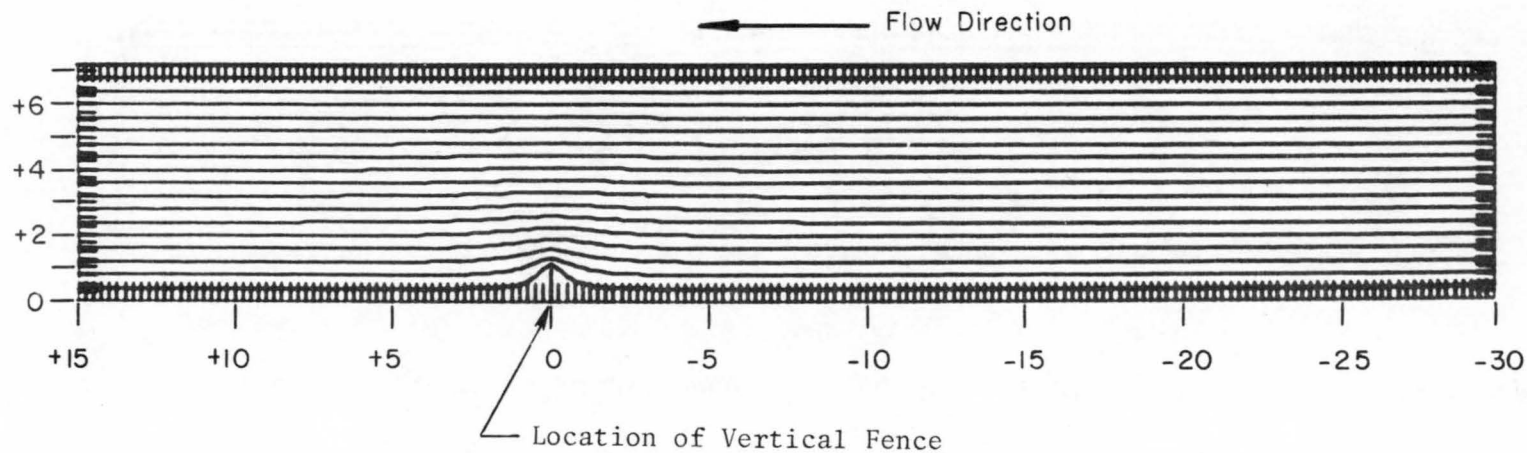
Contour From -4.500E+00 to 3.000E-01 Contour Interval of 3.000E-01
Scaled By 1E+02 Pt(3.3) = -8.924E-03

Temperature



Contour From 0. To 7.200E+00 Contour Interval of 4.000E-01
Scaled By 1E+02 Pt(3.3) = 4.930E-01

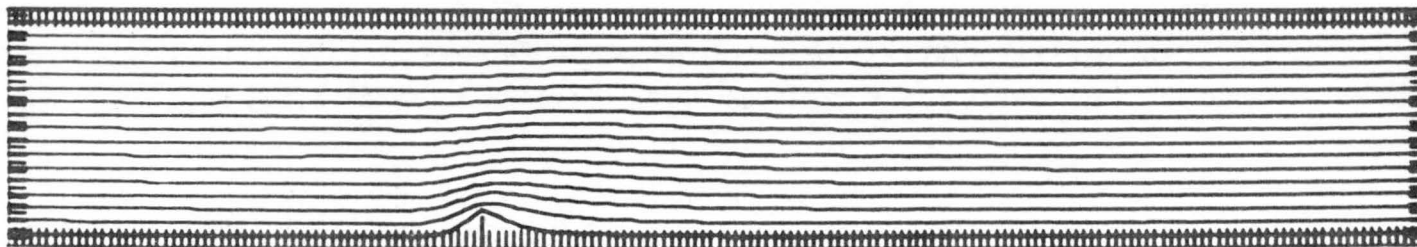
Fig. 14. Flow Patterns At $t = 15.68$, $Re = 397$, $Pr = 10$, $Ri = 1.58$,
 $\Delta X = 0.25$, $\Delta Z = 0.25$, $\Delta t = 0.20$, grid points (180 x 30)



Contour From 0. To 7.200E+00 Contour Interval of 4.000E-01
 Scaled By 1E+02 Pt(3.3) = 5.000E-01

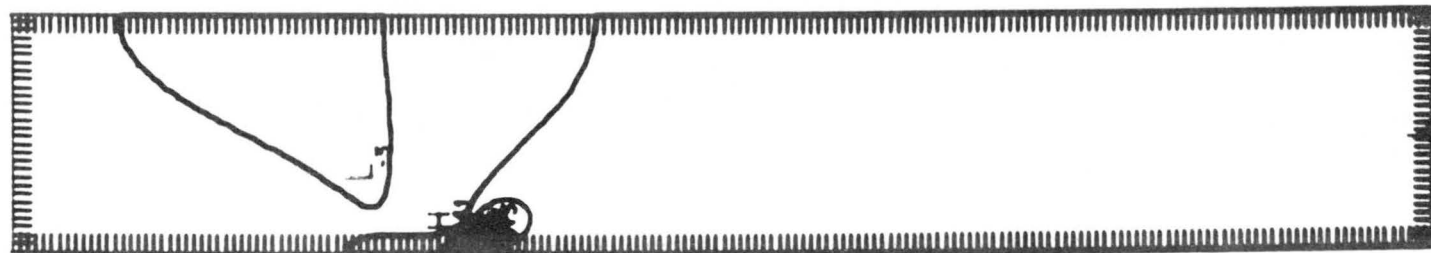
Fig. 15. Stream Function At $t = 0.03$, $Re = 5000$, $Pr = 1$, $Ri = 1.58$,
 $\Delta X = 0.25$, $\Delta Z = 0.25$, $\Delta t = 0.03$, grid points (180 x 30)

Stream
Function



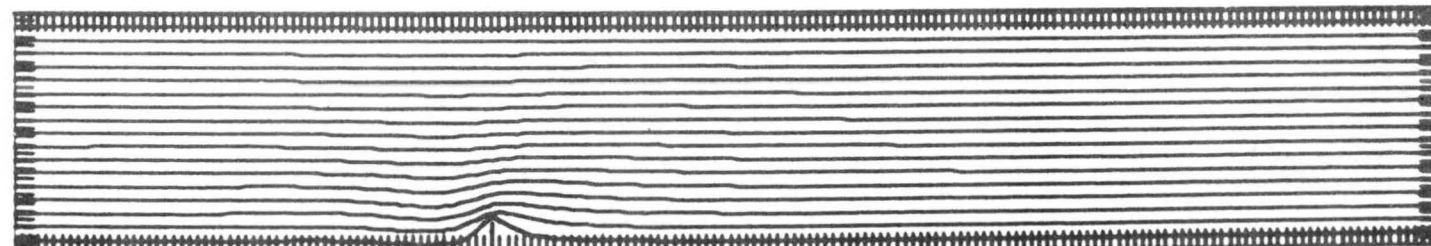
Contour From 0. To $7.200E+00$ Contour Interval of $4.000E-01$
Scaled by $1E+02$ Pt(3.3) = $5.000E-01$

Vorticity



Contour From $-5.100E+00$ to $3.000E-01$ Contour Interval of $3.000E-01$
Scaled by $1E+02$ Pt(3.3) = $-2.411E-06$

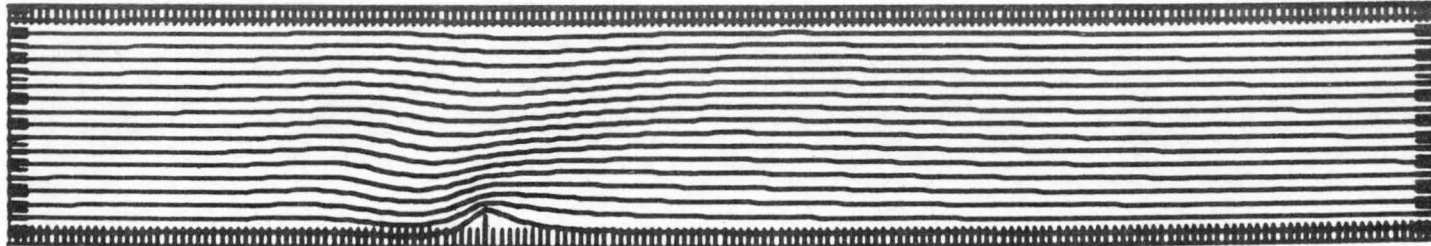
Temperature



Contour from 0. to $7.200E+00$ Contour Interval of $4.000E-01$
Scaled By $1E+02$ Pt(3.3) = $5.000E-01$

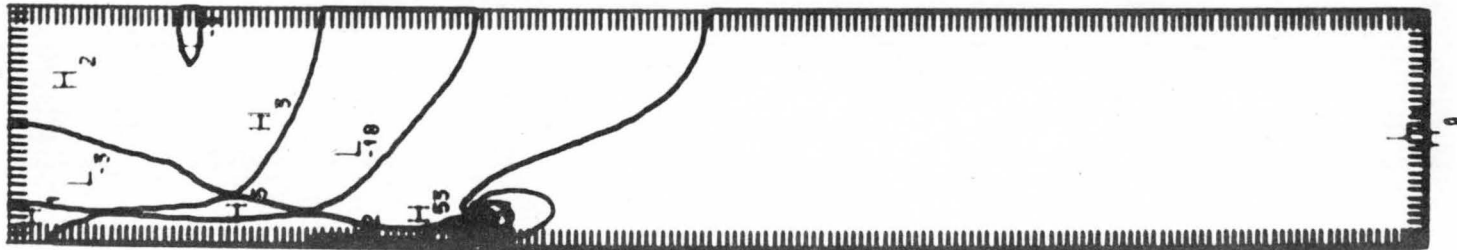
Fig. 16. Flow Patterns At $t = 2.88$, $Re = 5000$, $Pr = 1$, $Ri = 1.58$,
 $\Delta X = 0.25$, $\Delta Z = 0.25$, $\Delta t = 0.22$, grid points (180 x 30)

Stream
Function



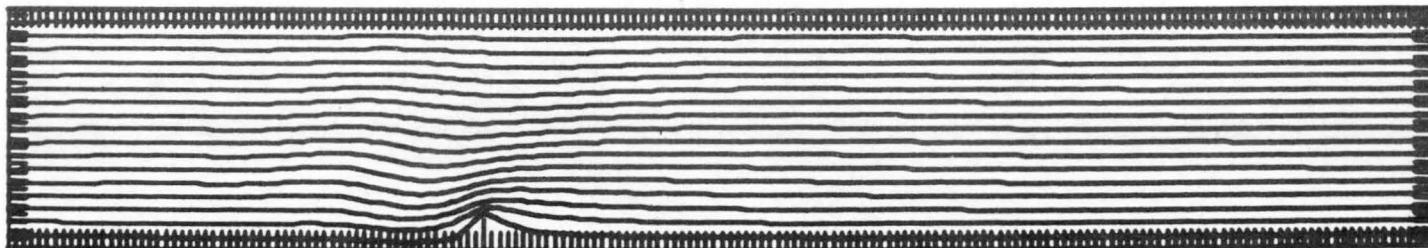
Contour From 0. To 7.200E+00 Contour Interval of 4.000E-01
Scaled By 1E+02 Pt(3.3) = 4.997E-01

Vorticity



Contour From -5.100E+00 to 3.000E-01 Contour Interval of 3.000E-01
Scaled By 1E+02 Pt(3.3) = -2.560E-04

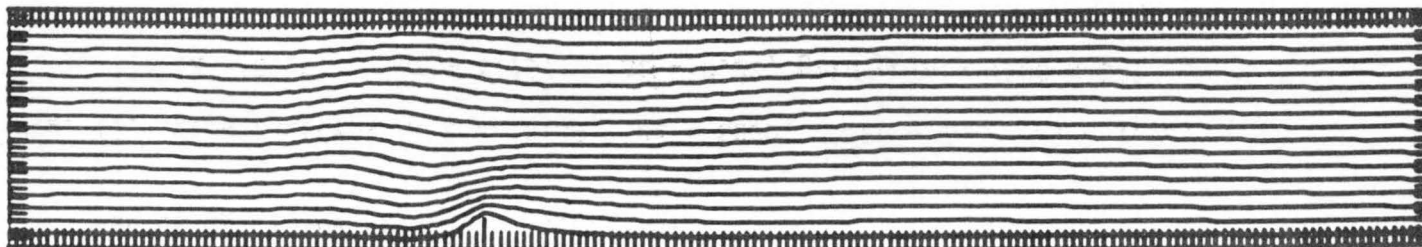
Temperature



Contour From 0. To 7.200E+00 Contour Interval of 4.000E-01
Scaled By 1E+02 Pt(3.3) = 4.998E-01

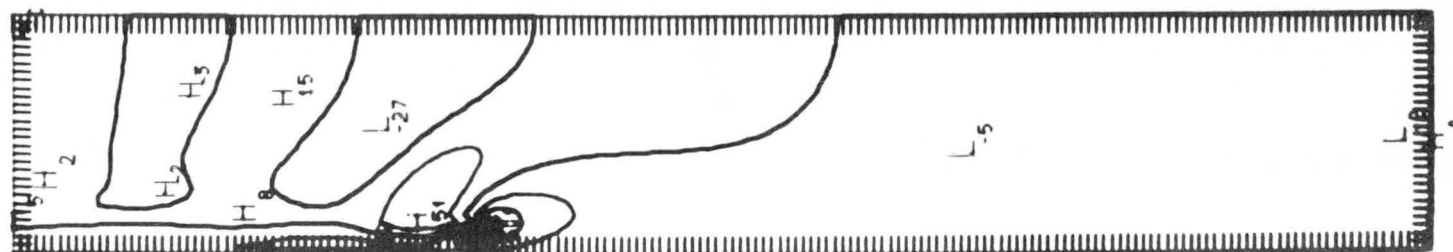
Fig. 17. Flow Patterns At $t = 8.34$, $Re = 5000$, $Pr = 1$, $Ri = 1.58$,
 $\Delta X = 0.25$, $\Delta Z = 0.25$, $\Delta t = 0.22$, grid points (180 x 30)

Stream
Function



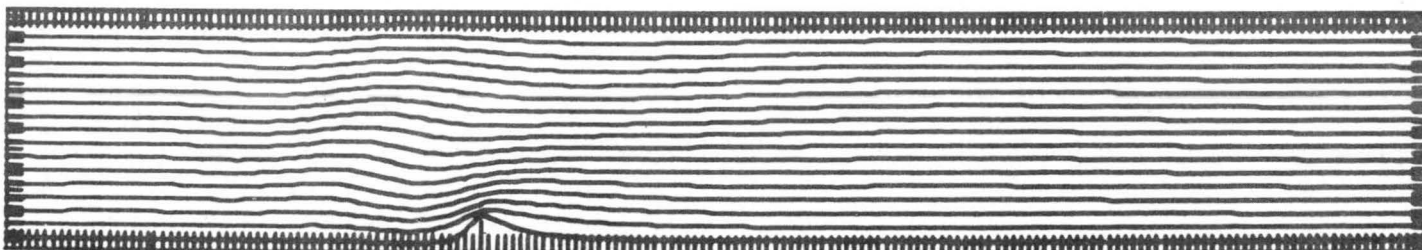
Contour From 0. To 7.200E+00 Contour Interval of 4.000E-01
Scaled By 1E+02 Pt(3.3) = 4.963E-01

Vorticity



Contour From -4.800E+00 To 3.000E-01 Contour Interval of 3.000E-01
Scaled By 1E+02 Pt(3.3) = -3.539E-03

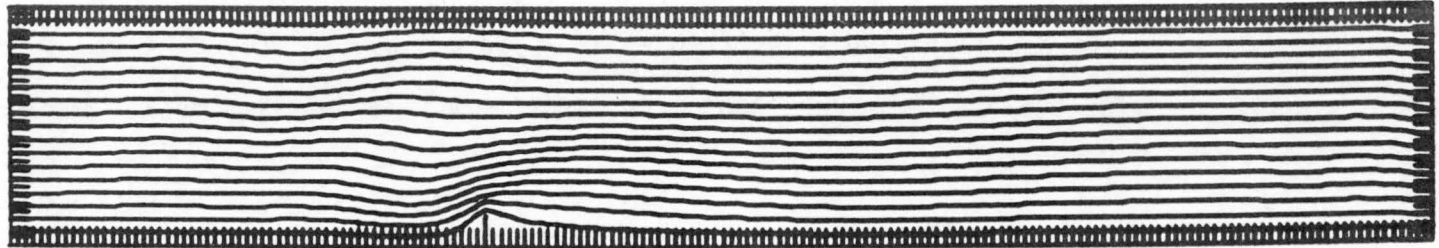
Temperature



Contour From 0. To 7.200E+00 Contour Interval of 4.000E-01
Scaled By 1E+02 Pt(3.3) = 4.972E-01

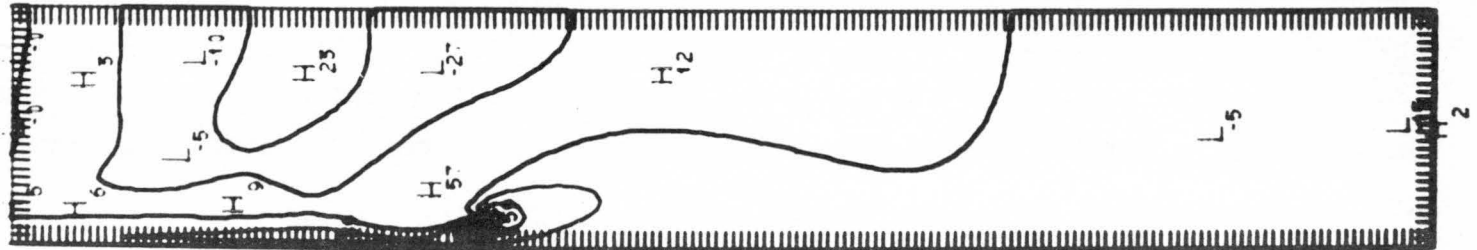
Fig. 18. Flow Patterns At $t = 13.38$, $Re = 5000$, $Pr = 1$, $Ri = 1.58$,
 $\Delta X = 0.25$, $\Delta Z = 0.25$, $\Delta t = 0.22$, grid points (180 x 30)

Stream
Function



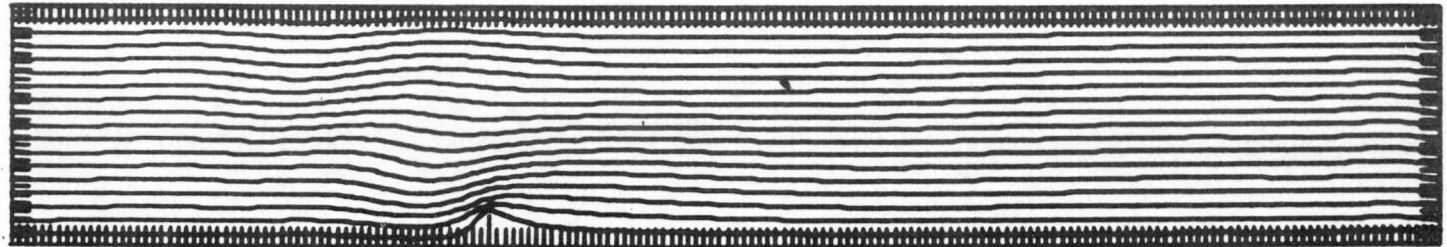
Contour From 0. To 7.200E+00 Contour Interval of 4.000E-01
Scaled By 1E+02 Pt(3.3) = 4.824E-01

Vorticity



Contour From -4.500E+00 To 3.000E-01 Contour Interval of 3.000E-01
Scaled By 1E+02 Pt(3.3) = -1.795E-02

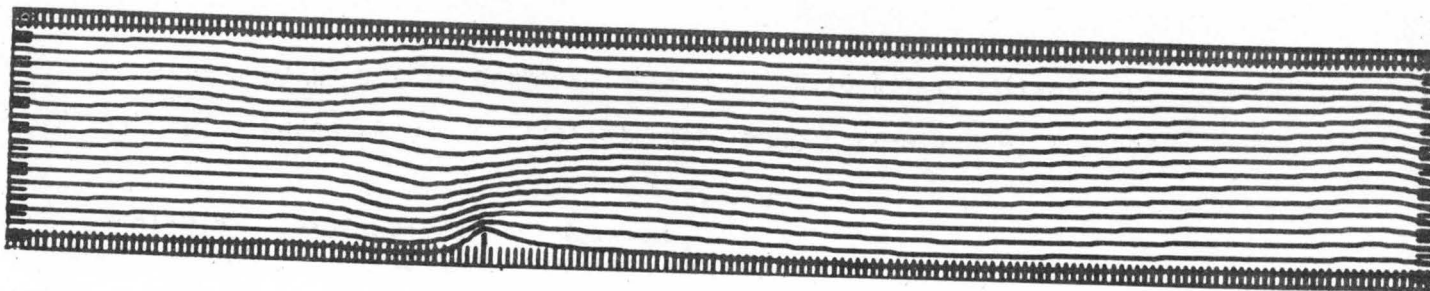
Temperature



Contour From 0. To 7.200E+00 Contour Interval of 4.000E-01
Scaled By 1E+02 Pt(3.3) = 4.862E-01

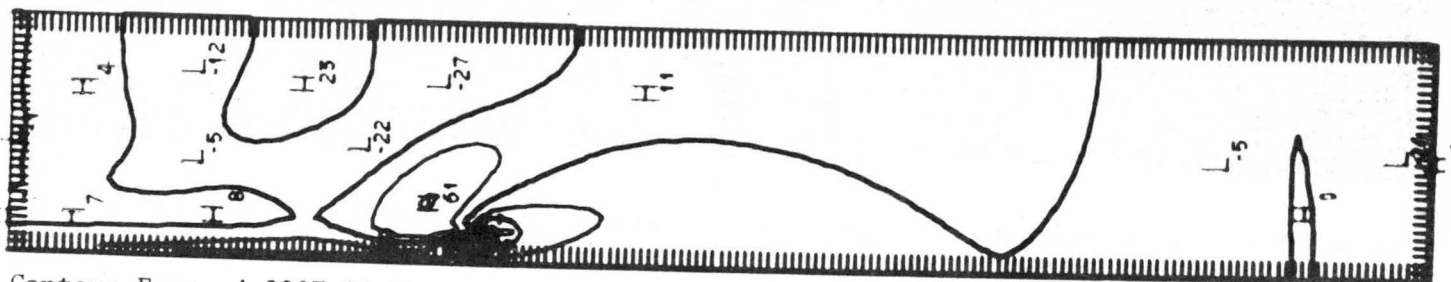
Fig. 19. Flow Patterns At $t = 18.42$, $Re = 5000$, $Pr = 1$, $Ri = 1.58$,
 $\Delta X = 0.25$, $\Delta Z = 0.25$, $\Delta t = 0.22$, grid points (180 x 30)

Stream
Function



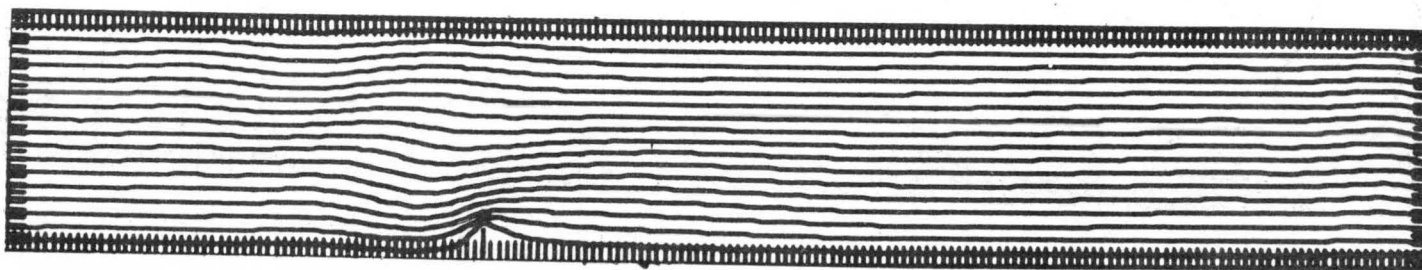
Contour From 0. To 7.200E+00 Contour Interval of 4.000E-01
Scaled By 1E+02 Pt(3.3) = 4.738E-01

Vorticity



Contour From -4.800E+00 To 6.000E-01 Contour Interval of 3.000E-01
Scaled By 1E+02 Pt(3.3) = -2.762E-02

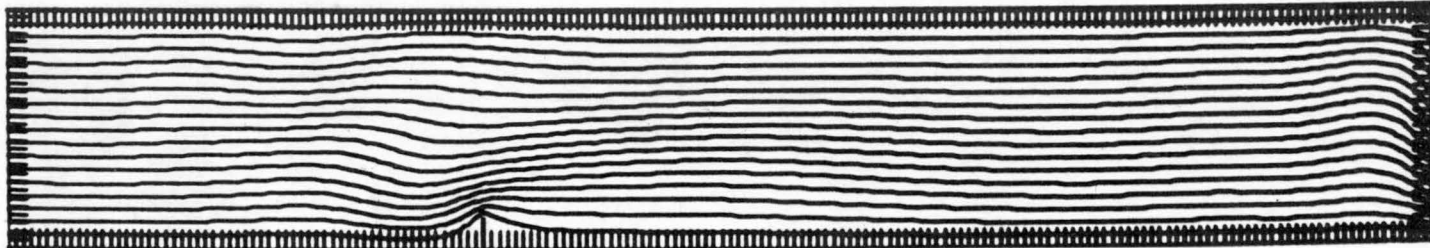
Temperature



Contour From 0. To 7.200E+00 Contour Interval of 4.000E-01
Scaled By 1E+02 Pt(3.3) = 4.791E-01

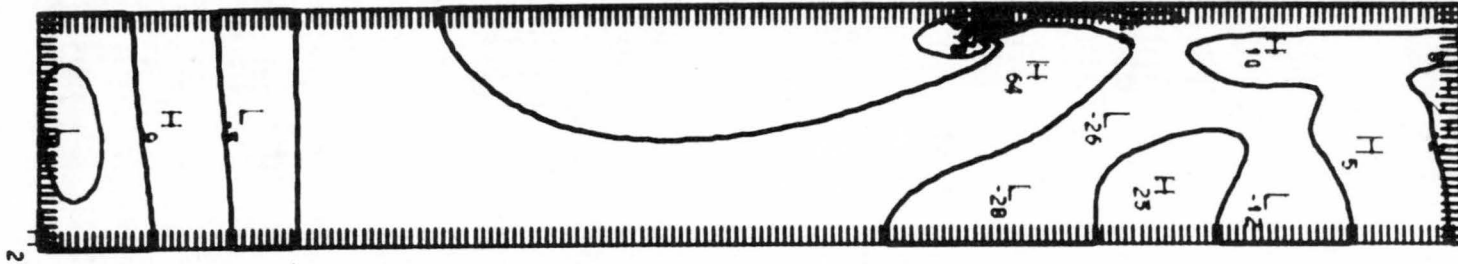
Fig. 20. Flow Patterns At $t = 20.52$, $Re = 5000$, $Pr = 1$, $Ri = 1.58$,
 $\Delta X = 0.25$, $\Delta Z = 0.25$, $\Delta t = 0.22$, grid points (180 x 30)

Stream
Function



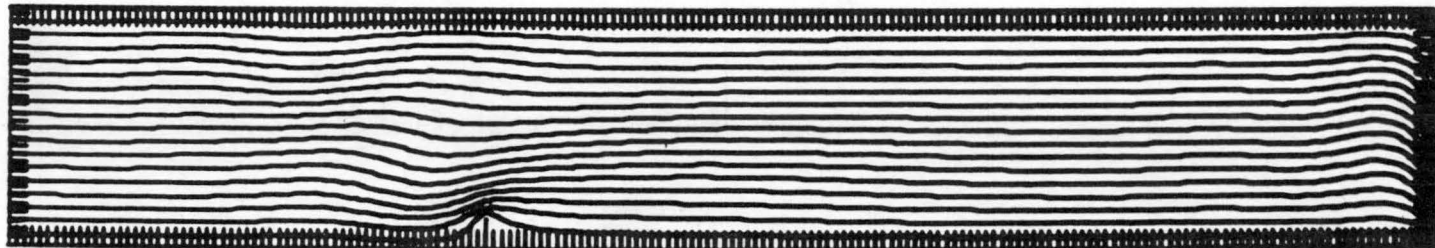
Contour From 0. To 7.200E+00 Contour Interval of 4.000E-01
Scaled By 1E+02 Pt(3.3) = 6.056E-01

Vorticity



Contour From -5.600E+00 to 4.000E-01 Contour Interval of 4.000E-01
Scaled By 1E+02 Pt(3.3) = -1.320E-01

Temperature



Contour From 0. To 7.200E+00 Contour Interval of 4.000E-01
Scaled By 1E+02 Pt(3.3) = 5.854E-01

Fig. 21. Flow Patterns At $t = 23.46$, $Re = 5000$, $Pr = 1$, $Ri = 1.58$,
 $\Delta X = 0.25$, $\Delta Z = 0.25$, $\Delta t = 0.22$, grid points (180 x 30)

DOCUMENT CONTROL DATA - R&D

(Security classification of title, body of abstract and indexing annotation must be entered when the overall report is classified)

1. ORIGINATING ACTIVITY (Corporate author) Fluid Dynamics & Diffusion Laboratory College of Engineering, Colorado State Univ. Fort Collins, Colorado 80521		2a. REPORT SECURITY CLASSIFICATION Unclassified
		2b. GROUP
3. REPORT TITLE Stratified Flow Over an Obstacle; A numerical Experiment		
4. DESCRIPTIVE NOTES (Type of report and inclusive dates) Technical Report		
5. AUTHOR(S) (Last name, first name, initial) LIN, Jung-Tai, and C. J. APELT		
6. REPORT DATE January 1970	7a. TOTAL NO. OF PAGES 94	7b. NO. OF REFS 22
8a. CONTRACT OR GRANT NO. N00014-68-A-0493 PROJECT NO. NR 062-414/6-6-68 (CODE 438)	9a. ORIGINATOR'S REPORT NUMBER(S) CER69-70JTL-CJA25	
c. d.	9b. OTHER REPORT NO(S) (Any other numbers that may be assigned this report) THEMIS TECHNICAL REPORT NO. 7	
10. AVAILABILITY/LIMITATION NOTICES Distribution of this report is unlimited		
11. SUPPLEMENTARY NOTES	12. SPONSORING MILITARY ACTIVITY Office of Naval Research U.S. Department of Defense Washington, D. C.	
13. ABSTRACT Numerical studies of time-dependent, two-dimensional, stratified flow of incompressible, viscous, diffusive fluid are described. The particular physical problem which has been considered is that of stratified flow over a vertical fence when the motion is impulsively started from rest. Solutions have been calculated for the following two cases: $R_e = 397$, $P_r = 10$, $R_i = 1.58$; and $R_e = 5000$, $P_r = 1$, $R_i = 1.58$. The results are presented as contour plots of the flow variables, generated directly by the computer. A new iterative method was used for numerical integration of the governing equations and was found to be very effective. The method is based on the combination of the Crank-Nicolson method with a strongly implicit iterative method developed by Stone (1968). Full details of the method are given together with a summary of its performance on the problems calculated. It is shown that proper treatment of the inflow and outflow boundary conditions is crucial for successful numerical modeling of stratified flows.		

14. KEY WORDS	LINK A		LINK B		LINK C	
	ROLE	WT	ROLE	WT	ROLE	WT
Stratified Flow Numerical Experiment Time-dependent Incompressible Viscous Diffusive Fluid Iterative Method						

INSTRUCTIONS

1. **ORIGINATING ACTIVITY:** Enter the name and address of the contractor, subcontractor, grantee, Department of Defense activity or other organization (*corporate author*) issuing the report.

2a. **REPORT SECURITY CLASSIFICATION:** Enter the overall security classification of the report. Indicate whether "Restricted Data" is included. Marking is to be in accordance with appropriate security regulations.

2b. **GROUP:** Automatic downgrading is specified in DoD Directive 5200.10 and Armed Forces Industrial Manual. Enter the group number. Also, when applicable, show that optional markings have been used for Group 3 and Group 4 as authorized.

3. **REPORT TITLE:** Enter the complete report title in all capital letters. Titles in all cases should be unclassified. If a meaningful title cannot be selected without classification, show title classification in all capitals in parenthesis immediately following the title.

4. **DESCRIPTIVE NOTES:** If appropriate, enter the type of report, e.g., interim, progress, summary, annual, or final. Give the inclusive dates when a specific reporting period is covered.

5. **AUTHOR(S):** Enter the name(s) of author(s) as shown on or in the report. Enter last name, first name, middle initial. If military, show rank and branch of service. The name of the principal author is an absolute minimum requirement.

6. **REPORT DATE:** Enter the date of the report as day, month, year; or month, year. If more than one date appears on the report, use date of publication.

7a. **TOTAL NUMBER OF PAGES:** The total page count should follow normal pagination procedures, i.e., enter the number of pages containing information.

7b. **NUMBER OF REFERENCES:** Enter the total number of references cited in the report.

8a. **CONTRACT OR GRANT NUMBER:** If appropriate, enter the applicable number of the contract or grant under which the report was written.

8b, 8c, & 8d. **PROJECT NUMBER:** Enter the appropriate military department identification, such as project number, subproject number, system numbers, task number, etc.

9a. **ORIGINATOR'S REPORT NUMBER(S):** Enter the official report number by which the document will be identified and controlled by the originating activity. This number must be unique to this report.

9b. **OTHER REPORT NUMBER(S):** If the report has been assigned any other report numbers (*either by the originator or by the sponsor*), also enter this number(s).

10. **AVAILABILITY/LIMITATION NOTICES:** Enter any limitations on further dissemination of the report, other than those imposed by security classification, using standard statements such as:

- (1) "Qualified requesters may obtain copies of this report from DDC."
- (2) "Foreign announcement and dissemination of this report by DDC is not authorized."
- (3) "U. S. Government agencies may obtain copies of this report directly from DDC. Other qualified DDC users shall request-through _____."
- (4) "U. S. military agencies may obtain copies of this report directly from DDC. Other qualified users shall request through _____."
- (5) "All distribution of this report is controlled. Qualified DDC users shall request through _____."

If the report has been furnished to the Office of Technical Services, Department of Commerce, for sale to the public, indicate this fact and enter the price, if known.

11. **SUPPLEMENTARY NOTES:** Use for additional explanatory notes.

12. **SPONSORING MILITARY ACTIVITY:** Enter the name of the departmental project office or laboratory sponsoring (*paying for*) the research and development. Include address.

13. **ABSTRACT:** Enter an abstract giving a brief and factual summary of the document indicative of the report, even though it may also appear elsewhere in the body of the technical report. If additional space is required, a continuation sheet shall be attached.

It is highly desirable that the abstract of classified reports be unclassified. Each paragraph of the abstract shall end with an indication of the military security classification of the information in the paragraph, represented as (TS), (S), (C), or (U).

There is no limitation on the length of the abstract. However, the suggested length is from 150 to 225 words.

14. **KEY WORDS:** Key words are technically meaningful terms or short phrases that characterize a report and may be used as index entries for cataloging the report. Key words must be selected so that no security classification is required. Identifiers, such as equipment model designation, trade name, military project code name, geographic location, may be used as key words but will be followed by an indication of technical context. The assignment of links, rules, and weights is optional.

February 1969

APPROVED DISTRIBUTION LIST FOR UNCLASSIFIED TECHNICAL
REPORTS ISSUED UNDER CONTRACT N00014-68-A-0493-0001
NR 062-414

Technical Library, Building 313
Aberdeen Proving Ground
Aberdeen, Maryland 21005

Dr. F. D. Bennett
Exterior Ballistics Laboratory
Ballistics Research Laboratories
Aberdeen Proving Ground
Aberdeen, Maryland 21005

Mr. C. C. Hudson
Sandia Corporation
Sandia Base
Albuquerque, New Mexico 87115

Defense Documentation Center
Cameron Station
Alexandria, Virginia 22314 (20)

Professor Bruce Johnson
Engineering Department
Naval Academy
Annapolis, Maryland 21402

Library
Naval Academy
Annapolis, Maryland 21402

Professor W. W. Willmarth
Department of Aerospace Engineering
University of Michigan
Ann Arbor, Michigan 48108

Professor A. Kuethe
Department of Aeronautical Engineering
University of Michigan
Ann Arbor, Michigan 48108

AFOSS (SREM)
1400 Wilson Boulevard
Arlington, Virginia 22209

Dr. J. Menkes
Institute for Defense Analyses
400 Army-Navy Drive
Arlington, Virginia 22204

M. J. Thompson
Defense Research Laboratory
University of Texas
P. O. Box 8029
Austin, Texas 78712

Library
Aerojet-General Corporation
6352 N. Irwindale Avenue
Azusa, California 91702

Professor S. Corsin
Department of Mechanics
Johns Hopkins University
Baltimore, Maryland 21218

Professor M. V. Morkovin
Aeronautics Building
Johns Hopkins University
Baltimore, Maryland 21218

Professor O. M. Phillips
Division of Mechanical Engineering
Institute for Cooperative Research
Johns Hopkins University
Baltimore, Maryland 21218

Geophysical Research Library
Air Force Cambridge Research Center
Bedford, Massachusetts 01731

Librarian
Department of Naval Architecture
University of California
Berkeley, California 94720

Professor Paul Lieber
Department of Mechanical Engineering
University of California
Berkeley, California 94720

Professor J. Johnson
412 Hesse Hall
University of California
Berkeley, California 94720

Professor A. K. Oppenheim
Division of Mechanical Engineering
University of California
Berkeley, California 94720

Professor M. Holt
Division of Aeronautical Sciences
University of California
Berkeley, California 94720

Dr. L. Talbot
Department of Engineering
Berkeley, California 94720

Professor R. J. Emrich
Department of Physics
Lehigh University
Bethlehem, Pennsylvania 18015

Engineering Library
Plant 25
Grumman Aircraft Engineering Corporation
Bethpage, Long Island, New York 11714

Mr. Eugene F. Baird
Chief of Dynamic Analysis
Grumman Aircraft Engineering Corporation
Bethpage, Long Island, New York 11714

Library
Naval Weapons Center
China Lake, California 93555

Library MS 60-3
NASA Lewis Research Center
21000 Brookpark Road
Cleveland, Ohio 44133

Professor J. M. Burgers
Institute for Fluid Dynamics and
Applied Mathematics
University of Maryland
College Park, Maryland 20742

Professor J. R. Weske
Institute for Fluid Dynamics and
Applied Mathematics
University of Maryland
College Park, Maryland 20742

Professor Pai
Institute for Fluid Dynamics and
Applied Mathematics
University of Maryland
College Park, Maryland 20742

NASA Scientific and Technical
Information Facility
Acquisitions Branch (S-AK/DL)
P. O. Box 33
College Park, Maryland 20740

Professor Loren E. Bollinger
The Ohio State University
Box 3113 - University Station
Columbus, Ohio 43210

Professor G. L. von Eschen
Department of Aeronautical and
Astronautical Engineering
Ohio State University
Columbus, Ohio 43210

Computations and Analysis Laboratory
Naval Weapons Laboratory
Dahlgren, Virginia 22448

Technical Library
Naval Weapons Laboratory
Dahlgren, Virginia 22418

Dr. J. Harkness
LTV Research Center
Ling-Temco-Vought Aerospace Corporation
P. O. Box 5907
Dallas, Texas 75222

Mr. Adolf Egli
Ford Motor Company
Engineering and Research Staff
P. O. Box 2053
Dearborn, Michigan 48123

School of Applied Mathematics
Indiana University
Bloomington, Indiana 47401

Commander
Boston Naval Shipyard
Boston, Massachusetts 02129

Director
Office of Naval Research Branch Office
495 Summer Street
Boston, Massachusetts 02210

Professor M. S. Uberoi
Department of Aeronautical Engineering
University of Colorado
Boulder, Colorado 80303

Technical Library
Naval Applied Science Laboratory
Building 1, Code 222
Flushing & Washington Avenues
Brooklyn, New York 11251

Professor J. J. Foody
Chairman, Engineering Department
State University of New York
Maritime College
Bronx, New York 10465

Mr. F. Dell'Amico
Cornell Aeronautical Laboratory
P. O. Box 235
Buffalo, New York 14221

Professor G. Birkhoff
Department of Mathematics
Harvard University
Cambridge, Massachusetts 02138

Professor B. Budiansky
Department of Mechanical Engineering
School of Applied Sciences
Harvard University
Cambridge, Massachusetts 02138

Dr. Ira Dyer
Bolt, Beranek and Newman, Inc.
50 Moulton Street
Cambridge, Massachusetts 02138

Department of Naval Architecture
and Marine Engineering
Massachusetts Institute of Technology
Cambridge, Massachusetts 02139

Professor Patrick Leehey
Department of Naval Architecture and
Marine Engineering
Massachusetts Institute of Technology
Cambridge, Massachusetts 02139

Professor E. Mollo-Christensen
Department of Aeronautics and Astronautics
Massachusetts Institute of Technology
Cambridge, Massachusetts 02139

Professor A. T. Ippen
Department of Civil Engineering
Massachusetts Institute of Technology
Cambridge, Massachusetts 02139

Professor C. C. Lin
Department of Mathematics
Massachusetts Institute of Technology
Cambridge, Massachusetts 02139

Professor H. C. Hottel
Department of Chemical Engineering
Massachusetts Institute of Technology
Cambridge, Massachusetts 02139

Commanding Officer
NROTC and Naval Administrative Unit
Massachusetts Institute of Technology
Cambridge, Massachusetts 02139

Professor R. F. Probst
Department of Mechanical Engineering
Massachusetts Institute of Technology
Cambridge, Massachusetts 02139

Technical Library
Webb Institute of Naval Architecture
Glen Cove, Long Island, New York 11542

Library, MS185
NASA Langley Research Center
Langley Station
Hampton, Virginia 23365

Dr. B. N. Pridmore Brown
Northrop Corporation
Norair-Division
Hawthorne, California 90250

Dr. J. P. Breslin
Davidson Laboratory
Stevens Institute of Technology
Hoboken, New Jersey 07030

Mr. D. Savitsky
Davidson Laboratory
Stevens Institute of Technology
Hoboken, New Jersey 07030

Mr. S. Tsakonias
Davidson Laboratory
Stevens Institute of Technology
Hoboken, New Jersey 07030

Professor J. F. Kennedy, Director
Iowa Institute of Hydraulic Research
University of Iowa
Iowa City, Iowa 52240

Professor L. Landweber
Iowa Institute of Hydraulic Research
University of Iowa
Iowa City, Iowa 52240

Professor John R. Glover
Iowa Institute of Hydraulic Research
University of Iowa
Iowa City, Iowa 52240

Professor E. L. Resler
Graduate School of Aeronautical
Engineering
Cornell University
Ithaca, New York 14851

Technical Library
Scripps Institution of Oceanography
University of California
La Jolla, California 92037

Professor S. R. Keim
University of California
Institute of Marine Resources
P. O. Box 109
La Jolla, California 92038

Dr. B. Sternlicht
Mechanical Technology Incorporated
968 Albany-Shaker Road
Latham, New York 12110

Mr. P. Eisenberg
HYDRONAUTICS, Incorporated
Pindell School Road
Howard County, Laurel, Maryland 20810

Technical Library
Charleston Naval Shipyard
Naval Base
Charleston, South Carolina 29408

Director
Office of Naval Research Branch Office
219 South Dearborn Street
Chicago, Illinois 60604

Technical Library
Puget Sound Naval Shipyard
Bremerton, Washington 98314

Technical Library
Annapolis Division
Naval Ship Research & Development Center
Annapolis, Maryland 21402

Code ESD-AROD
Army Research Office
Box CM, Duke Station
Durham, North Carolina 27706

Professor Ali Bulent Cambel
Chairman, Department of Mechanical
Engineering
Northwestern University
Evanston, Illinois 60201

Professor A. Charnes
The Technological Institute
Northwestern University
Evanston, Illinois 60201

Barbara Spence Technical Library
AVCO-Everett Research Laboratory
2385 Revere Beach Parkway
Everett, Massachusetts 02149

Dr. Martin Bloom
Director of Dynamics Research
Department of Aerospace Engineering
and Applied Mechanics
Polytechnic Institute of Brooklyn-
Graduate Center
Route 110
Farmingdale, New York 11201

Professor J. E. Cermak
Professor-in-Charge, Fluid Mechanics
Program
College of Engineering
Colorado State University
Fort Collins, Colorado 80521

Mr. Seymour Edelberg
Lincoln Laboratory
Massachusetts Institute of Technology
P. O. Box 73
Lexington, Massachusetts 02173

Technical Library
Long Beach Naval Shipyard
Long Beach, California 90801

Professor A. F. Charwat
Department of Engineering
University of California
Los Angeles, California 90024

Professor R. W. Leonard
University of California
Los Angeles, California 90024

Professor John Laufer
Department of Aerospace Engineering
University Park
University of California
Los Angeles, California 90007

Professor J. F. Ripkin
St. Anthony Falls Hydraulic Laboratory
University of Minnesota
Minneapolis, Minnesota 55414

Lorenz G. Straub Library
St. Anthony Falls Hydraulic Laboratory
University of Minnesota
Minneapolis, Minnesota 55414

Library
Naval Postgraduate School
Monterey, California 93940

Professor A. B. Metzner
Department of Chemical Engineering
University of Delaware
Newark, Delaware 19711

Technical Library
Navy Underwater Sound Laboratory
Port Trumbull
New London, Connecticut 06320

Technical Library
Naval Underwater Weapons Research
and Engineering Station
Newport, Rhode Island 02840

Professor W. J. Pierson, Jr.
Department of Meteorology and
Oceanography
New York University
University Heights
New York, New York 10405

Professor J. J. Stoker
Courant Institute of Mathematical
Sciences
New York University
251 Mercer Street
New York, New York 10003

Engineering Societies Library
345 East 47th Street
New York, New York 10017

Office of Naval Research
New York Area Office
207 W. 24th Street
New York, New York 10011

Commanding Officer
Office of Naval Research Branch Office
Box 39, FPO, New York 09510 (25)

Professor A. G. Strandhagen
Department of Engineering, Mechanics
University of Notre Dame
Notre Dame, Indiana 46556

Miss O. M. Leach, Librarian
National Research Council
Aeronautical Library
Montreal Road
Ottawa 7, Canada

Lockheed Missiles and Space Company
Technical Information Center
3251 Hanover Street
Palo Alto, California 94301

Professor M. S. Plesset
Engineering Science Department
California Institute of Technology
Pasadena, California 91109

Professor H. W. Liepmann
Department of Aeronautics
California Institute of Technology
Pasadena, California 91109

Dr. Jack W. Hoyt (Code P2501)
Associate Head, Ocean Technology
Department
Naval Undersea Warfare Center
3202 E. Foothill Blvd.
Pasadena, California 91107

Dr. F. R. Hama
Jet Propulsion Laboratory
4800 Oak Grove Drive
Pasadena, California 91103

Professor T. Y. Wu
Division of Engineering
California Institute of Technology
Pasadena, California 91109

Professor A. J. Acosta
Department of Mechanical Engineering
California Institute of Technology
Pasadena, California 91109

Director
Office of Naval Research Branch Office
1030 E. Green Street
Pasadena, California 91101

Professor F. Zwicky
Department of Physics
California Institute of Technology
Pasadena, California 91109

Dr. E. E. Sechler
Executive Officer for Aeronautics
California Institute of Technology
Pasadena, California 91109

Dr. R. H. Kraichnan
Dublin, New Hampshire 03444

Technical Library (Code 249b)
Philadelphia Naval Shipyard
Philadelphia, Pennsylvania 19112

Dr. Sinclair M. Scala
Space Sciences Laboratory
General Electric Company
P. O. Box 8555
Philadelphia, Pennsylvania 19101

Dr. Paul Kaplan
Oceanics, Inc.
Technical Industrial Park
Plainview, L. I., New York 11803

Technical Library
Naval Missile Center
Point Mugu, California 93041

Technical Library
Portsmouth Naval Shipyard
Portsmouth, New Hampshire 03801

Technical Library
Norfolk Naval Shipyard
Portsmouth, Virginia 23709

Professor G. W. Duvall
Department of Physics
Washington State University
Pullman, Washington 99164

Chief, Document Section
Redstone Scientific Information Center
Army Missile Command
Redstone Arsenal, Alabama 35809

Professor M. Lessen, Head
Department of Mechanical Engineering
University of Rochester
College of Engineering, River
Campus Station
Rochester, New York 14627

Dr. H. N. Abramson
Southwest Research Institute
8500 Culebra Road
San Antonio, Texas 78228

Editor
Applied Mechanics Review
Southwest Research Institute
8500 Culebra Road
San Antonio, Texas 78206

Dr. S. L. Zieberg, Head
Gas Dynamics Section, Fluid Mechanics
Building B-1, Room 1320
Aerospace Corporation
San Bernardino, California 92402

Mr. Myles B. Berg
Aerospace Corporation
P. O. Box 1308
San Bernardino, California 92402

Mr. W. B. Barkley
General Dynamics Corporation
Electric Boat Division
Marine Technology Center, P. O. Box 911
San Diego, California 92112

Library (128-000)
CONVAIR - Division of General Dynamics
P. O. Box 12009
San Diego, California 92112

Technical Library
Pearl Harbor Naval Shipyard
Box 400, PPO, San Francisco 96610

Technical Library, Code H245C-3
Hunters Point Division
San Francisco Bay Naval Shipyard
San Francisco, California 94135

Office of Naval Research San Francisco
Area Office
1076 Mission Street
San Francisco, California 94103

Gail T. Flesher - 44
GM Defense Research Laboratory
Box T
Santa Barbara, California 93102

Library
The RAND Corporation
1700 Main Street
Santa Monica, California 90401

Dr. H. T. Nagamatsu
General Electric Company
Research and Development Center K-1
P. O. Box 8
Schenectady, New York 12301

Fenton Kennedy Document Library
The Johns Hopkins University
Applied Physics Laboratory
8621 Georgia Avenue
Silver Spring, Maryland 20910

Chief, Library Division
Naval Ordnance Laboratory
White Oak
Silver Spring, Maryland 20910

Dr. R. E. Wilson
Associate Technical Director
(Aeroballistics)
Naval Ordnance Laboratory
White Oak
Silver Spring, Maryland 20910

Aerophysics Division
Naval Ordnance Laboratory
White Oak
Silver Spring, Maryland 20910

Dr. A. E. Seigel
Naval Ordnance Laboratory
White Oak
Silver Spring, Maryland 20910

Dr. S. Kline
Mechanical Engineering 501 G
Stanford University
Stanford, California 94305

Engineering Library
Department 218, Building 101
McDonnell Aircraft Corporation
P. O. Box 516
St. Louis, Missouri 63166

Mr. R. W. Kermeen
Lockheed Missiles & Space Company
Department 57101, Building 150
Sunnyvale, California 94086

Professor S. Eskinazi
Department of Mechanical Engineering
Syracuse University
Syracuse, New York 13210

Professor J. Poa
Department of Aeronautical Engineering
Rensselaer Polytechnic Institute
Troy, New York 12180

Professor R. C. DiPrima
Department of Mathematics
Rensselaer Polytechnic Institute
Troy, New York 12180

Professor L. M. Milne-Thomson
Mathematics Department
University of Arizona
Tucson, Arizona 85721

Dr. E. J. Skudrzyk
Ordnance Research Laboratory
Pennsylvania State University
University Park, Pennsylvania 16801

Dr. M. Sevik
Ordnance Research Laboratory
Pennsylvania State University
University Park, Pennsylvania 16801

Dr. G. F. Wislicenus
Ordnance Research Laboratory
Pennsylvania State University
University Park, Pennsylvania 16801

Dr. A. S. Iberall, President
General Technical Services, Inc.
8794 West Chester Pike
Upper Darby, Pennsylvania 19082

Dr. J. M. Robertson
Department of theoretical and
Applied Mechanics
University of Illinois
Urbana, Illinois 61803

Shipyard Technical Library
Code 130L7, Building 746
San Francisco Bay Naval Shipyard
Vallejo, California 94592

Commander
Naval Ship Research and Development Center
Attn: Code 513 (1)
Code 901 (1)
Code 942 (1)
Code 01 (Dr. Powell) (1)
Code 042 (1)
Code 520 (1)
Code 800 (1)
Washington, D. C. 20007

Commander
Naval Ship System Command
Attn: Technical Library (2052) (1)
Washington, D. C. 20360

Director, Engineering Science Division
National Sciences Foundation
Washington, D. C. 20550

Chief of Naval Research
Department of the Navy
Attn: Code 438 (3)
Code 461 (1)
Code 463 (1)
Code 468 (1)
Code 421 (1)
Washington, D. C. 20360

Commander
Naval Air Systems Command
Department of the Navy
Attn: Code AIR 370 (1)
Code AIR 6042 (1)
Washington, D. C. 20360

Librarian Station 5-2
Coast Guard Headquarters
1300 E Street, N. W.
Washington, D. C. 20226

Division of Engineering
Maritime Administration
441 G Street, N. W.
Washington, D. C. 20235

Commander
Naval Oceanographic Office
Washington, D. C. 20390

Code 2027
Naval Research Laboratory (6)
Washington, D. C. 20390

Science and Technology Division
Library of Congress
Washington, D. C. 20540

Commander
Naval Ordnance Systems Command
Attn: ORD 913 (Library) (1)
ORD 035 (1)
Washington, D. C. 20360

Library
National Bureau of Standards
Washington, D. C. 20234

Chief of Research and Development
Office of Chief of Staff
Department of the Army
The Pentagon, Washington, D. C. 20310

Dr. Frank Lane
General Applied Science Laboratory
Merrick and Stewart Avenues
Westbury, Long Island, New York 11590

Director
Woods Hole Oceanographic Institute
Woods Hole, Massachusetts 02543

Mr. W. J. Mykytow
AF Flight Dynamics Laboratory
Wright-Patterson Air Force Base
Ohio 45433

Dr. H. Cohen
IBM Research Center
P. O. Box 218
Yorktown Heights, New York 10598